University of CRETE

Department of MATERIALS SCIENCE & TECHNOLOGY

Design & Study of Self-Assembled Bio-inorganic materials

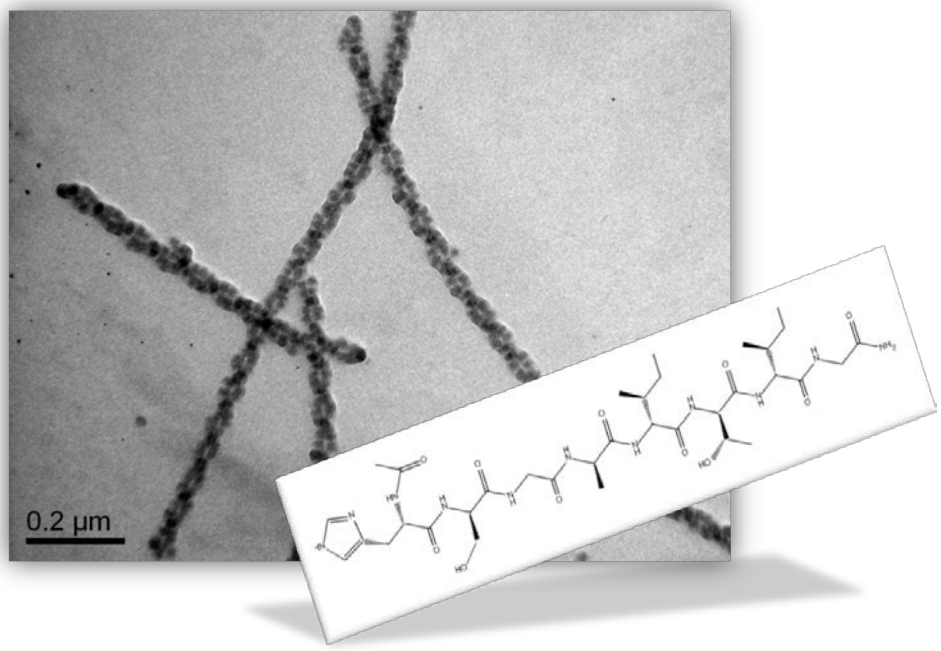

Master Thesis: Anagnostopoulou Evangelia – Eleni

Supervisor: Assoc. Prof. Anna Mitraki

January 2013

Abstract

The present thesis is based in the use of self-assembling peptides as templates for directing formation of inorganic materials. This kind of "biomimetic" approach is based on the ability of biological materials and especially proteins and peptides to act as templates for the deposition of inorganic materials in various natural processes. Such processes include the formation of calcium phosphates in bone and teeth morphogenesis, calcium carbonates in nacre formation, and biosilica formation in sponges. Biosilica formation in sponges involves the protein silicatein, an homolog of the cathepsin family of proteases. The catalytic center of silicateins involves a "catalytic triad" (Ser, His and Asn) that is able to hydrolyse silicon alkoxides in vitro to yield Si hydroxide, followed by polycondensation to form the metal oxide network material.

In our group, it was previously demonstrated that self-assembling octapeptides that contain serine residues in second position from a free amino terminus (eg NH_2-NSGAITIG-$CONH_2$) are able to direct silica deposition [Kasotakis, E., E. Mossou, et al. (2009). "Design of Metal-Binding Sites Onto Self-Assembled Peptide Fibrils." Biopolymers 92(3): 164-172]. The underlying mechanism was demonstrated and involves activation of the serine residue by the free amino terminus. This mechanism is analogue to the mechanism adopted by a special class of serine proteases, called N-terminal hydrolases. In the present thesis we will show that another self-assembling octapeptide, Ac-HS-GAITIG-$CONH_2$ is able to direct silica deposition. We examined the ability of the Ac-HS-GAITIG-$CONH_2$ building block to self-assemble into amyloid-like fibers and then the functionality of the serine and histidine residues in the process. We finally show that the arrangement of the silica nanoparticles on the fibril follows the geometry of the underlying fibril template.

Acknowledgments

I would like to express my deepest appreciation to my supervisor, Assoc. Prof. Anna Mitraki, whose guidance and persistent help encouraged me to accomplish this dissertation. Except for imparting me her knowledge, she conveyed me a spirit of excitement for research regarding the world of self-assembled peptides.

I would like to thank my committee members, Assoc. Prof. Maria Vamvakaki and Assistant Prof. Kelly Velonia, whose educational work during my master program broadened my scientific knowledge and way of thinking.

It gives me a great pleasure acknowledging the hospitality and freedom to carry out experiments at the "Supramolecular Chemistry and Biomaterials" lab of Prof. Kelly Velonia. Special thanks to MSc Eleftheria Daskalaki for her technical support and funny moments. A part of this thesis would not be possible to be accomplished without the suggestions and expertise of Dr. Manolis Kasotakis from the institute of "Biology and Technology" of Saclay in Paris.

It was a great honor to collaborate with the staff of the Electron Microscopy Facility "Vassilis Galanopoulos", Alexandra Siakouli, Aleka Manousaki, Dimitris Theodoridis and Stefanos Papadakis. Their expertise helped me to set up a big part of my thesis.

I am indebted to my colleagues Assist. Prof. Maria Chatzinikolaidou, MSc Chrystalleni Hadjicharalambous, MSc Ariadni Prigipaki, MSc Konstantina Terzaki, MSc Destpoina Katsougri, Vaggelis Georgilis for the team work, exchange of ideas and being good friends.

Finally, I would like to thank my parents Vangelis and Maria for their vital encouragement in every critical step of my life.

INDEX

List of figures and tables

CHAPTER 1 Introduction

1.1 Nanotechnology & supramolecular chemistry

A major step in science during the 21st century was the introduction of nanotechnology, a multidisciplinary field, which combines biology, chemistry and physics. It was in 1959 when the physicist Richard Feynman at his lecture "There's plenty of room at the bottom – An invitation to enter a new field of physics" established nanotechnology, even if he did not really mention the term. During his speech he emphasized to the great progress in biology and suggested that scientists should mimic the efficiency of cells in being very active and tiny at the same time. Inspired by cells functionality and their ability to store information he proposed them as a model for technological applications. Thus the field of supramolecular biochemistry came into light where molecular building blocks interact with non-covalent bonds (table 1.1) and through a "bottom-up" arrangement form supramolecular entities. This self-organization is the central theme of the so called "building blocks of life", for example nucleic acid bases and amino acids, which join together and form assemblies of a characteristic morphology and functionality.

Attractive Force	Repulsive Force
Van der waals	Steric
Solvation	Solvation
Hydrophobic	Hydration
π-π stacking	Electric double-layer
Hydrophobic	
Bridging	
Deplition	
Coordination bond	

Table 1.1 Non-covalent forces that contribute to supramolecular "bottom-up" arrangement of building blocks (from Yoon S. Lee, 2008).

1.2 Fibrous proteins and their building blocks

Fibrous proteins are self-assembling systems of great interest, because they result on supramolecular structures of outstanding strength and flexibility. Their properties stem from their secondary structure, where individual amino acid sequences act as building blocks for the formation of "rod-like" entities. These polypeptide repeating sets run parallel to each other and very often are linked by disulphide cross bridges making the protein elongated and strong. They can be distinguished into 3 categories regarding their structure:

a – helical fibrous proteins

a keratins are found in hair, nails and horns of mammals. Their building block is a polypeptide sequence of a 7-residue repeat which forms two a-helices twisted around each other resulting to a coiled coil (dimer). In the center of each coil there are two non polar residues, while cysteine amino acids participate in disulfide bridges that cross-link neighboring coiled-coils to build up a filament. The N and C-terminal domains of each polypeptide facilitate the assembly of coiled coils into protofilaments, two of which constitute a protofibril. The self-assembly of four protofibrils results in a microfibril, which associates with other microfibrils to form a macrofibril (Charlotte W. Pratt et al., 2009).

For example, Laminin EGF protein is a component of membranes and takes part in cell differentiation, growth and adhesion. It consists of three chains which are cross-linked by disulphide bonds and form a coiled coil structure (Jean D. Sipe, 2005). Each helix in its first half is based on the repetition of 60 amino acids (polypeptide building block) that includes eight conserved Cys (http://www.ebi.ac.uk/interpro/IEntry?ac=IPR002049):

xxCxCxxxxxxxxxxxxCxxxxxxxCxxCxxxxxGxxCxxCxxgaagxxxxxxxxxxxCxx

Fig 1.1 Polypeptide building block in the laminin protein, where C the conserved Cys involved in a disulphide bond, a aromatic residue, g conserved Gly (from http://www.ebi.ac.uk/interpro/IEntry?ac=IPR002049)

β – sheet fibrous proteins

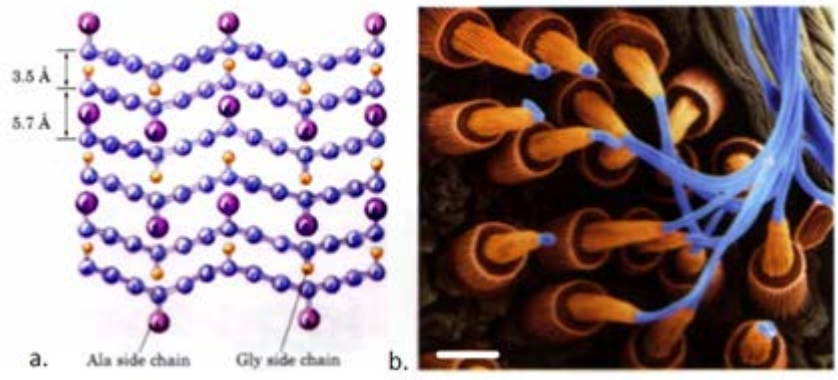

Fig 1.2 Structure of silk. a. Antiparallel β sheets rich in Ala (or Ser) (purple) and Gly (yellow) amino acids, b. electron micrograph where strands of fibroin (blue) emerge from the spinnerets of a spider (scale bar 70μm), (Nelson and Cox, 2000).

Silk fibroin: Fibers are found in the silk produced by insects and spiders for the formation of cocoons, nests and webs. Silk fibroin from *Bombyx mori* is the protein which is the result of the "bottom-up" arrangement of the 6-residue sequence: Gly-Ser-Gly-Ala-Gly-Ala. These amino acids associate into antiparallel β strands which extend parallel to the fiber axis. The high concentration in glycine (45%) and alanine (30%), leads to a tight packing of sheets which contributes to the high rigidity of silk fibers (fig. 1.2). Finally, silk is flexible because neighboring beta sheets associate only through relatively weak van der Waals forces.

Elastin is a connective tissue protein responsible for the elasticity of soft tissues and organs. The subunit of elastin is tropoelastin, a combination of large hydrophobic polypeptide chains consisting of 33% Gly, 10% Pro and Hyp, 23% Ala and 13% Val. The peptapeptide sequence Val-Pro-Gly-Val-Gly form hydrophobic regions that are thought to adopt a "beta-spiral" conformation and they are surrounded by regions rich in Ala and Lys. The Lys residues contribute to the formation of a cross-linked network.

Collagen class/triple helix

Collagen is the major component of connective tissues in all animals, such as skin, teeth, tendon and blood vessels. Its building block is a polypeptide chain of a 3-residue repeating sequence Gly-X-Y, where where X is often Pro, and Y is often Hyp. Three parallel chains form helices which twist around each other giving a triple-helical structure called tropocollagen. This close packing is further stabilized by van der Waals interactions and extensice hydrogen bonding (Charlotte W. Pratt et al., 2009).

Fibers originating from Adenovirus

Adenovirus fibers are a distinct category of fibrous proteins that originate from adenoviruses responsible for respiratory, gastrenteric and ocular inflexions. Adenoviruses are icosahedral capsids with trimeric fiber shafts protruding from each of the 12 vertices. Van Raaij et al. (van Raaij, Mitraki et al. 1999) found that the human serotype 2 fiber shaft consists of a N-terminal tail (43 residues), a monomer of 15-residue pseudo-repeats (43-397 residues, hydrophobic amino acids alternating with hydrophilic and Gly or Pro at concerved positions) and a C-terminal head (397-582) (fig. 1.3). Each monomer folds into a β-strand parallel to the fiber axis, followed by a β-turn and a β-strand.

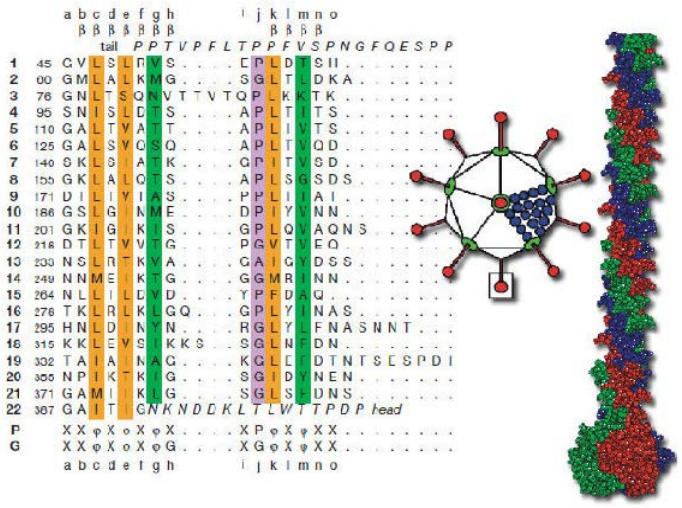

Fig. 1.3 (from left to right) Adenovirus fiber shaft sequence (where ϕ and X symbolizes hydrophobic and any type of residues respectively), adenovirus capsid and fiber shaft (from (van Raaij, Mitraki et al. 1999)

CHAPTER 2 Amyloid-like fibrils

2.1 Amyloid proteins

In contrast to the previously mentioned functional fibrous self-assemblies, a class of fibers, called amyloid fibrils is often associated with pathologies. These structures are responsible for a plethora of diseases such as type 2 diabetes, medullary carcinoma of the thyroid and Alzheimer's (Sipe and Cohen 2000).

Islet amyloid (AIAPP) is a 37 amino acid hormone detected in patients with type 2 diabetes. In vitro studies, (Westermark, Wernstedt et al. 1987) found that AIAPP has the tendency to form amyloid structures through a rapid transition from β-sheets. Later they (Tenidis, Waldner et al. 2000) showed that the penta- and hexapeptide $hIAPP_{23-27}$ (FGAIL) and $hIAPP_{22-27}$ (NFGAIL) can also form amyloid fibrils. Kayed et al. (Kayed, Bernhagen et al. 1999), also proved the β-sheet origin of amyloid fibrils using as building block the peptide IAPP.

Human calcitonin hCT hormone is a polypeptide associated with the medullary carcinoma of the thyroid. Its amyloid character is based on the "bottom-up" self-assembly of the peptides DFNKF and DFNK.

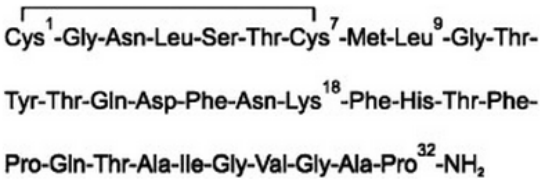

Fig. 2.1 Human calcitonin sequence (hCT). The N-terminus is stabilized by a disulfide bridge between Cys^1 and Cys^7, the C-terminus is naturally amidated.

Amyloid β-peptide (Aβ) is a 42 aa peptide found in neurofibrillary tangles and amyloid plaques of Alzheimer's disease. The heptapeptide KLVFFAE, corresponding to residues 16-22 residues, self-assembles into β-sheets and then into higher fibrilar structures. This sequence is thought to be a crucial building block in the self-assembly of the amyloid peptide (Gilead and Gazit 2005).

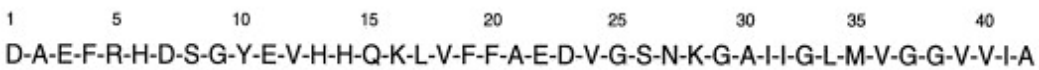

Fig. 2.2 Amyloid β-peptide (Aβ) sequence (Gilead and Gazit 2005).

2.2 Criteria for an amyloid-like structure

As it can be seen all amyloid fibrils that have been studied present the same structural motif, which can be used in order to fabricate novel amyloid-like structures. These must follow the characteristics of amyloid fibrils:

Typically, the building block of an amyloid fibril is a polypeptide chain (β-strand) organized in an almost fully extended conformation, where the axial distance between adjacent amino acids is 3.5Å. When two or more β-strands are linked by hydrogen bonds between N–H and C=O groups they form a β-sheet, called amyloid seed. β-sheets can be parallel, where the adjacent chains run in the same direction or antiparallel in the case they run in the opposite direction. If the side chain interactions between them and the medium permits, the amyloid seed self-organizes into thin filaments (protofibrils) of ~4-6 nm width and length<100nm. Protofibrils undergo a last assembly for the formation of a mature amyloid fibril with a characteristic cross β-sheet strucure (d~10 nm and l>1-10μm) (fig. 2.3).

All amyloid fibrils bind with the dye Congo red and give a green birefringence under cross-polarised light. The X-ray diffraction pattern reveals their cross β structure (i.e. strands perpendicular to the fibril axis) as well as the β-sheet self-assembly of their building blocks (fig. 2.4).

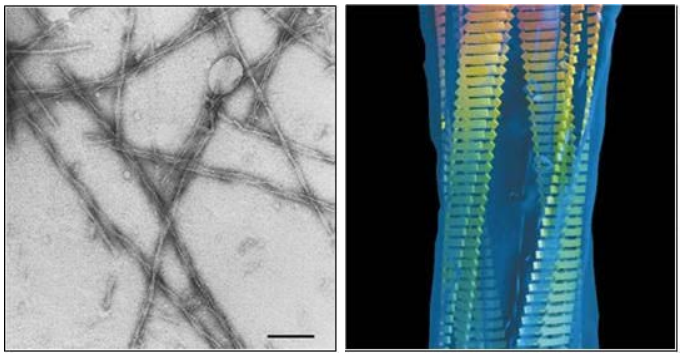

Fig. 2.3 TEM image of amyloid fibril and cross β-sheet structure (Dobson, 1999).

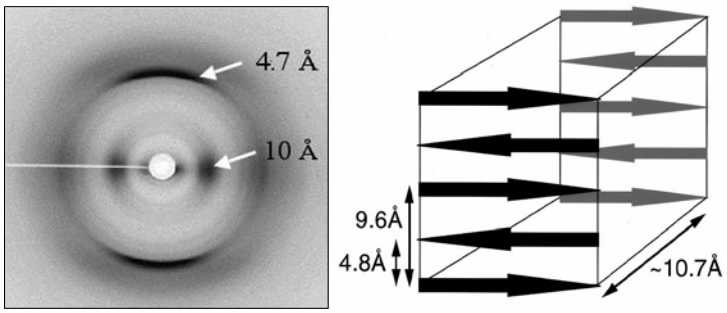

Fig. 2.4 Characteristic X-ray fibre diffraction pattern showing the cross-β amyloid structure. The reflection at 4.7Å corresponds to the hydrogen bonding distance between β-strands

and the 10Å indicates the distance between β-sheets. A reflection at 9.6Å reveals the presence of anti-parallel β-sheets (Serpell 2000).

2.3 Adenovirus fiber as a model for peptide assemblies

Luckey and Papanikolopoulou et al. synthesized poly- and oligopeptides (41aa, 25aa, 12aa, 8aa and 6 aa sequence, fig. 2.5) from the adenovirus fiber shaft in order to examine their structural characteristics (Luckey, Hernandez et al. 2000) (Papanikolopoulou, Teixeira et al. 2004). All peptides self-assembled into amyloid-like fibrils (fig. 2.6) and gave x-ray fiber diffractions of characteristic reflections, indicating their β-sheet conformation.

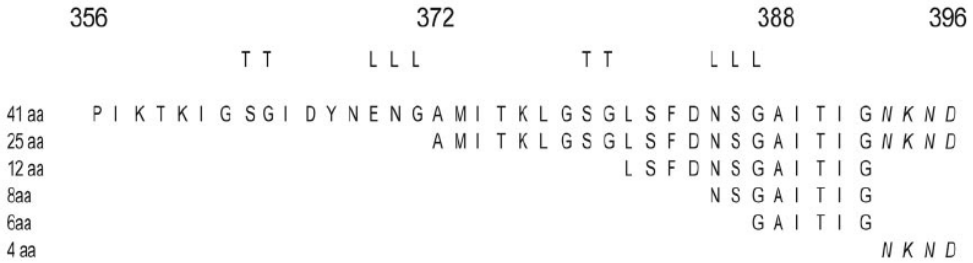

Fig. 2.5 Amino acid sequence from the human adenovirus serotype 2 fiber shaft (from (Papanikolopoulou, Teixeira et al. 2004)

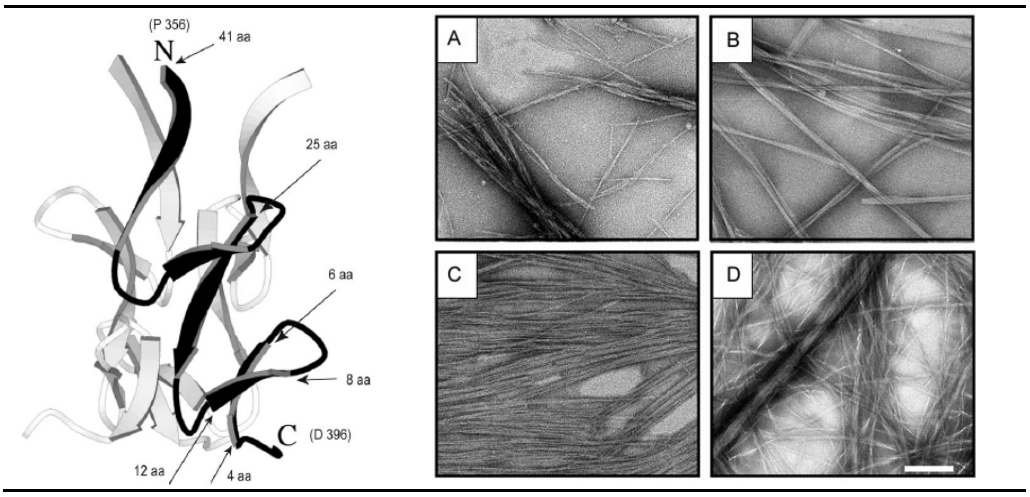

Fig. 2.6 Triple beta-spiral motif from the human adenovirus serotype 2 fiber shaft (left) and TEM images from the 25-, 12-, 8-, and 6-amino acid peptides (Papanikolopoulou, Schoehn et al. 2005).

The octapeptide NSGAITIG was further examined with transmission electron microscopy, atomic force microscopy and X-ray fiber diffraction. It forms amyloid-like fibers of 10nm diameter and some microns in length. According to the crystal structure of the native

protein the N-S-G residues are located at the loop and the A-I-T-I-G residues at the beta-strand. In order to explore the arrangement of amino acids in the fibrilar structure Tamamis et al. performed Molecular Dynamics Simulations (MDS) (Tamamis, Kasotakis et al. 2009). The simulations showed that the A-I-T-I (Ala-Ile-Thr-Ile) residues form a hydrophobic moiety of the cross beta amyloid core and the N-S residues form a type-II turn on the surface of fiber. The peptides were shown to prefer a parallel arrangement along the axis of the fibril.

2.4 Peptide hydrogels and their properties

A basic characteristic of nanofibril peptide assemblies is the spontaneous formation of 3-dimensional hybrid networks, which are called hydrogels. The density of these physical gels depends on the non-covalent interactions of peptides into the medium and the environmental conditions, such as temperature. There are two basic characteristics of peptide hydrogels, which make them appropriate for biotechnological and biomedical applications such as tissue engineering, drug delivery and microfluidics (Zhang, Skardal et al. 2008):

1. Biodegradability

The non covalent bonds between the fibrils of hydrogels make them compatible with various enzymatic or chemical biological functions due to their labile character (Hennink and van Nostrum 2002).

2. Biocompatibility

It has been proven that self-assembled peptide hydrogels are excellent scaffolds for cell attachment and proliferation, therefore they can be used in tissue engineering applications (Zhang 2003)

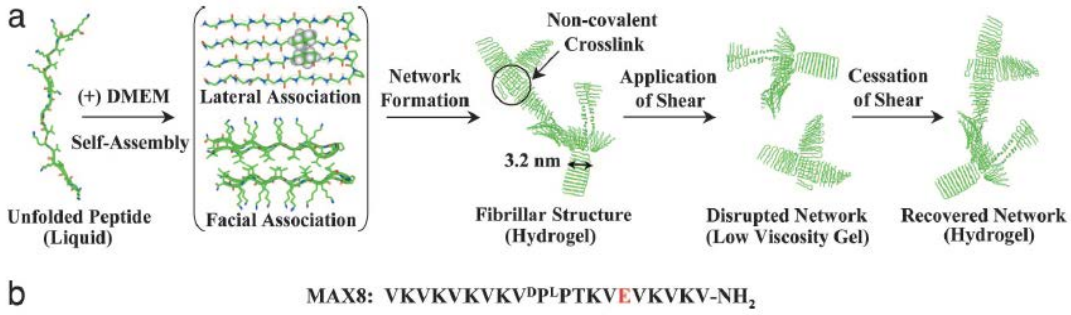

Fig. 2.7 Self-assembly, shear-thinning and self-healing mechanism of hydrogels. (*a*) The addition of DMEM of unfolded peptide induces formation a rigid hydrogel with a fibrillar structure. Application of shear stress disrupts the noncovalently stabilized network, leading

a low-viscosity gel. Upon cessation of shear, the network structure recovers to a rigid hydrogel again. *b*) Peptide sequence of MAX8 (from (Haines-Butterick, Rajagopal et al. 2007)

Such a biocompatible hydrogel peptide system was synthesized by Schneider et al. who used as a building block the peptide MAX8 (fig. 2.7b). This peptide was unfolded in a buffer solution of HEPES pH 7.4. However, after the addition of DMEM (pH 7.4, 37°C) it folded into β-hairpins (composed of two β-strand sequences of alternating hydrophobic and hydrophilic residues Lys and Val respectively) and self-assembled into a β-sheet-rich hydrogel (fig. 2.7a). (Haines-Butterick, Rajagopal et al. 2007). Also, Shuguang Zhang designed a 15-peptide with alternating positively and negatively charged amino acids, which self-assembles into an amyloid-like fibrillar hydrogel network (2.8) (Zhang 2003).

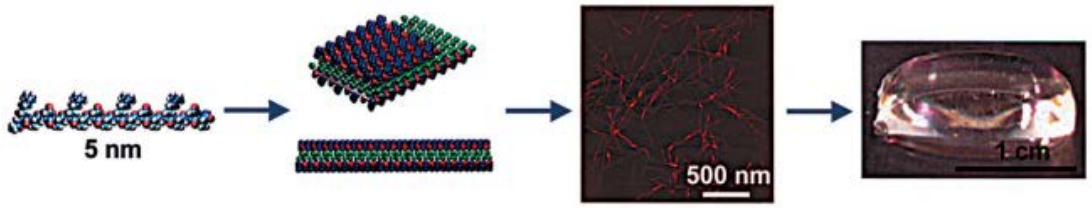

Fig. 2.8 Ionic self-complementary peptides forming hydrogel (non-polar residues are depicted in green, (+) and (-) charged residues are in blue and red respectively) (from (Zhang 2003).

2.5 Inorganic composites of self-assembling peptides

Self-assembling peptides were used as templates for the fabrication of metal nanostructures by several groups. Gazit et al. fabricated peptide hollow nanotubes by the dipeptide di-phenylalanine, allowing the entrance of silver ions and the subsequent formation of wires. For the removal of the peptide coating he used the enzyme proteinase K, revealing a silver wire of 20 nm diameter (fig. 2.9) (Reches and Gazit 2003).

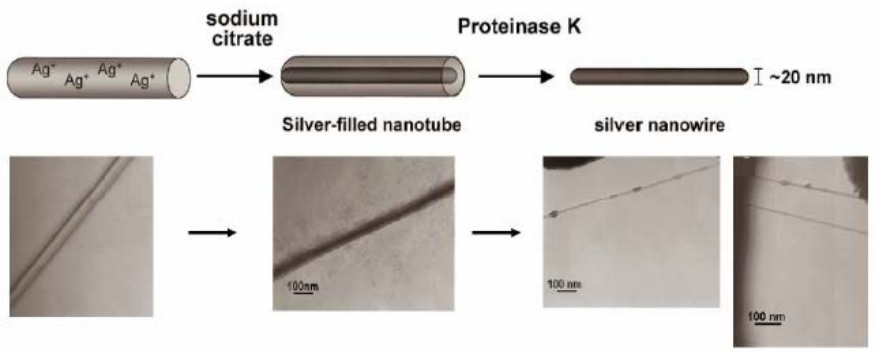

Fig. 2.9 Ionic silver is reduced to metallic silver within the tube lumen. The peptide coating is then removed by the use of enzymatic degradation (Reches and Gazit 2003).

Another example of bio-inorganic structure was introduced by Thomas Scheibel and Susan Lindquist. They used the N-terminal and middle region (NM) of yeast Saccharomyces cerevisiae which form self-assembling β-sheet-rich amyloid fibers. Since these structures were stable under a wide variety of harsh physical conditions, they were engineered for technological applications. The addition of a Cys residue upon fibers surface set them able for the nucleation and deposition of gold and silver nanoparticles of 100nm diameter (fig. 2.10) [Scheibel et al., 2003].

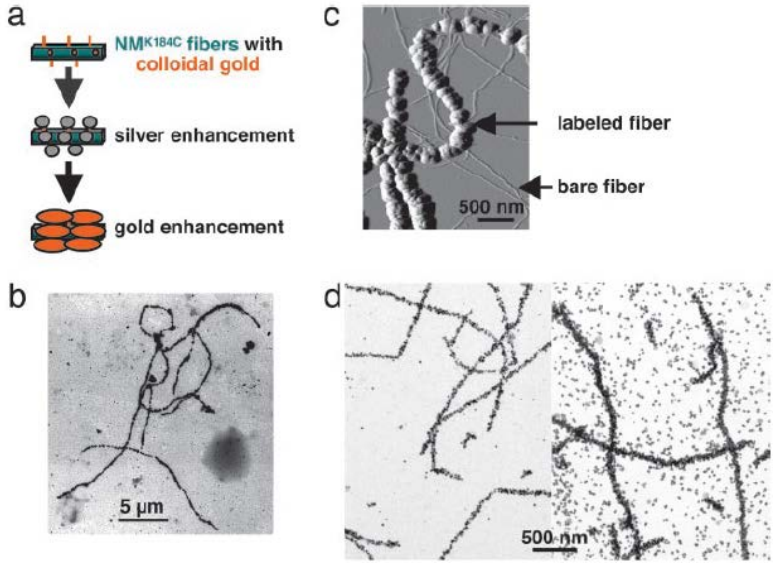

Fig. 2.10 Gold and silver coating of amyloid fibrils. a. The thiol side group of Cys binds with metals which are nucleated upon the surface of fibrils, b-d transmission electron images of gold and silver coated fibrils [Scheibel et al., 2003].

CHAPTER 3 Biosilification

3.1 Biosilification in diatoms and sponges

The last two decades a new, more ecological, approach has prevailed in industrial and research processes called "Green Chemistry". It is about a new way of thinking and acting in order to live in a more sustainable environment. Green Chemistry's philosophy promotes the use of alternative feedstocks and solvents, less dangerous reagents, the design of safer chemicals and products with minimum energy consumption by developing innovative reaction conditions which mimic natural processes.

In terms of global production, amorphous hydrated silicon dioxide $SiO_2 \cdot nH_2O$ (or opal) is the most abundant biomineral produced from primitive organisms and animals to higher plants. Their catalytic activity is based on proteins and peptides that are able to produce nano- and microstructures with high precision, in a large copy number & under mild physiological conditions. Since, chemical production of silica requires a combination of high temperature and pressure, extreme pH and the presence of caustic chemicals (Foo et al.), we will get inspired from natural proteins. Two of the most remarkable examples of biological silification are diatoms and sponges, where the process occurs under mild conditions of temperatures between 0-37^{o}C, neutral pH and ambient pressure. Below we will present the basic proteins that hydrolyze and template silica onto those organisms.

Diatoms

Diatoms are single-celled algae that inhibit in both marine and freshwater. The first attempt to understand the origin of silification was by Sumper and coworkers who isolated the cell wall (frustule) from Cylindrotheca fusiformis (fig. 3.1) (Sumper and Brunner 2006). Three groups of proteins were indentified: Frustulins, pleuralins and silaffins. Frustulis and pleuralins do not participate in silica catalysis, in contrast to silaffins which were further analyzed into three polypeptides: silaffin-1A, silaffin-1B and silaffin-2.

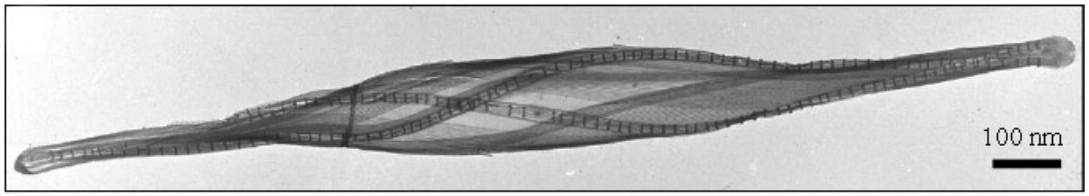

Fig. 3.1 Transmission electron image of the diatom Cylindrotheca fusiformis.

The cloning of silaffin gene (fig. 3.2) showed that it comprises of 3 parts: 1.A N-terminal domain, which is a typical amino acid sequence (1-19 amino acids), 2. A highly acidic area (20-107 amino acids) and 3. A C-terminal domain, composed by seven basic repeating units (R1-R7) rich in lysine and arginine. The peptides silaffin-1A and silaffin-1B are derived from R2–R7 and R1 sequences respectively.

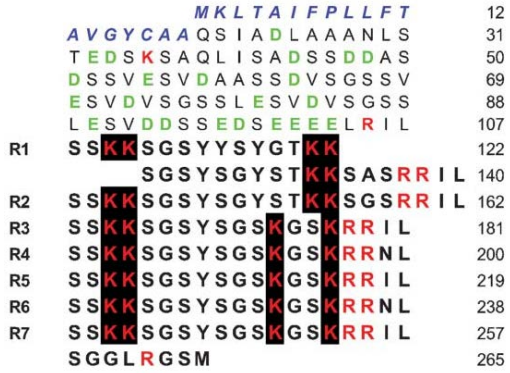

Fig. 3.2 Amino acid sequence of sil1p. Acidic amino acid residues are depicted in bold green and basic amino acid residues in bold red. The silaffin-generating C-terminal domain is shown in bold letters with boxed lysine residues 9 (Kroger, Deutzmann et al. 1999).

Several groups examined the precipitation activity of these domains as well as of their synthetic analogues. The polypeptide derived from the sequence R5 showed that in pH above 7 it could template silica from orthosilicic acid. Stone and colleagues further showed that the synthetic peptide based on the R5 region catalyzes silica formation from Tetramethoxysilane (TMOS) and creates remarkable morphologies of silica particles at the nanoscale. This is because R5 has a great number of Lys-Lys and Arg residues which interact electrostatically with the negatively silica nanoparticles and promote silica deposition (Naik, Whitlock et al. 2003), (Knecht and Wright 2003), (Wright, Teichmann et al. 2005), (Kroger, Deutzmann et al. 1999).

Sponges

Sponges, or Porifeans, are the oldest metazoans that use silica for the formation of their skeleton. Two classes of sponges, Demospongiae and Hexactinellida, have their mineral skeleton, called spicule, composed of hydrated amorphous silica that is formed in specifically

differentiated cells, the sclerocytes. Each spicule contains a central macroscopic organic core, or axial filament of protein, that is wholly included within the biosilica (fig. 3.3). The organic silica phase of siliceous spicules contains 6-13% H_2O, yielding an approximate formula of $(SiO_2)_{2\text{-}5}{\cdot}H_2O$. The axial filament of Demosponge consists of a protein, silicatein, which is enzymatically active and catalyzes the synthesis of silica from silicon alkoxides in vitro.

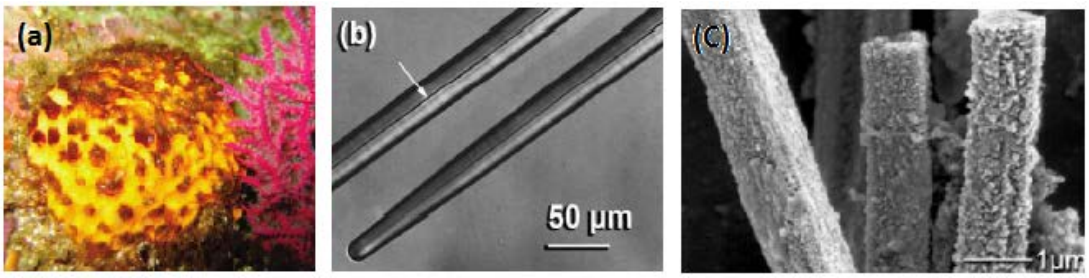

Fig. 3.3 (a) The marine sponge Tethya aurantia, (b) Optical micrographs of spicules from *Tethya auranti (*The higher magnification image in part b reveals the axial protein filaments (indicated by an arrow), *(c)* Scanning electron micrograph of the coated silicatein filaments after their reaction with TEOS (Brutchey, 2008 #671}.

3.2 Silicatein & its catalytic mechanism

Silicateins are members of the hydrolytic (cystein protease) enzymes –the cathepsin-L family proteases. The catalytic center (*cc*) of silicatein is comprised of the amino acids *Ser(26)*, *His (165)*, and *Asn (185)* (fig. 3.4 yellow color). There are two distinctive features of silicateins over cathepsins: in the catalytic center where the cysteine is replaced by a serine residue & the presence of a serine-rich cluster (green color) that plays a templating role in biosilification on enzyme's surface.

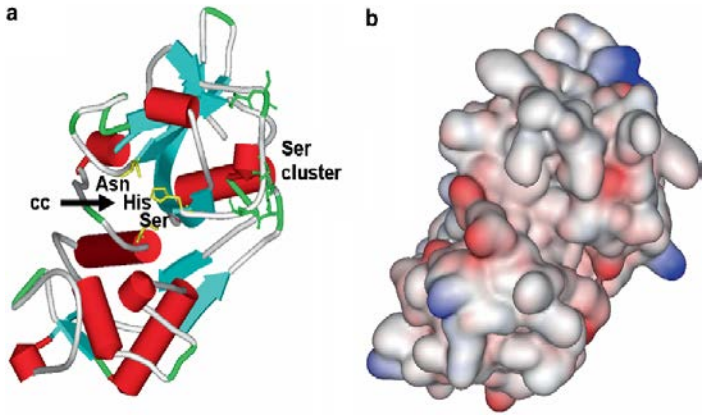

Fig. 3.4 Three-dimensional modeling of silicatein-α (*Suberites domuncula*). (**a**) Secondary structure elements are marked in *red* (α-helices) or *blue* (β-strands). (**b**) Electrostatic charge

distribution; *red*, positive charges; *blue*, negative charges; *white*, hydrophobic areas (from Heinz C. Schröder, 2009)

Silicatein's catalytic activity was examined in vitro by Morse et al. who used as a model substrate an ethyl ester of silicic acid, tetraethylorthosilicate (TEOS) in pH 7 (Brutchey and Morse 2008). As it can be seen in fig. 3.5 silicatein can successfully hydrolyse and deposit silica upon its surface. Even if TEOS is unknown in biological silification processes, it is proved to be a good precursor. This is due to the Si-OC bonds which are similar to a numerous conjugates of silicic acid during its reaction with intracellular ionophores and condensation with other biological molecules (Morse et al.). As far as the mechanism of silica hydrolysis and deposition is concerned, Perry and Tucker proposed the following steps:

1. Polycondensation/nucleation of silicic acid in order to form a stable nucleus.
2. Growth of the nucleus to form spherical particles (nano to micro scale) and
3. Aggregation/fusion of particles (Ostwald ripening) to form the spicules (Perry and Keeling-Tucker 2000)

In principle, four products containing free silanol groups can be formed by hydrolysis of TEOS: $Si(OC_2H_5)_3OH$, $Si(OC_2H_5)_2(OH)_2$, $Si(OC_2H_5)(OH)_3$ and $Si(OH)_4$ (silicic acid). The relative proportions and the kinetics of formation of these molecule species are unknown.

1. Nucleation

In the proposed silicatein – mediated reaction, the negatively charged Asn attracts the proton from the imidazole nitrogen and His becomes more powerful base. Through an electron transport the other imidazole nitrogen has an excess of electrons attracting the proton of Serine hydroxyl group. The nucleophilicity of serine oxygen facilitates its SN^2 type nucleophilic attack on the substrate silicon center (fig. 3.6). The elimination of ethanol follows and a transitory covalent protein-O-Si intermediate is formed. This intermediate is potentially stabilized by nitrogen donation from the imidazole to form a pentacoordinate silicon center. Addition of water will form silanole (Si-OH) completing the hydrolysis process (the oxygen of Ser attacks water's proton and then water's oxygen attacks to the substrate's Si). The formed silanol, $HOSi(OEt)_3$, reacts with another silicon substrate unit, $Si(OEt)_4$ (fig. 3.5) (Cha, Shimizu et al. 1999) (Shimizu, Cha et al. 1998)

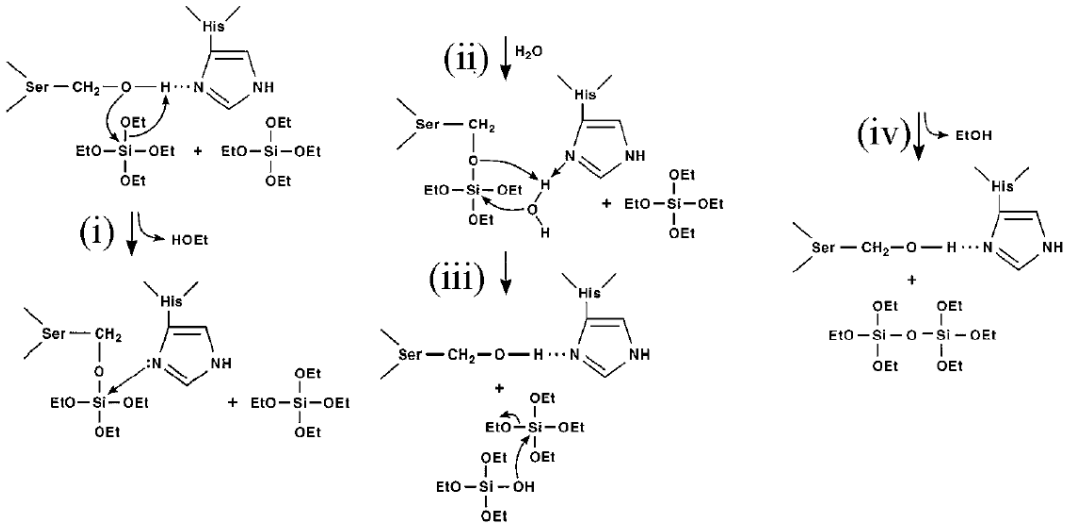

Fig. 3.5 Proposed TEOS polycondensation pathway from silicatein-enzyme active center (Cha et. al., 1999)

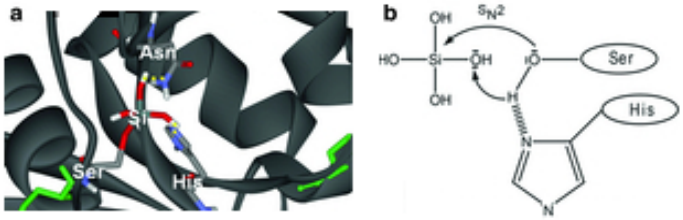

Fig. 3.6 (**a**) Detailed structure of silicatein-α showing the interaction of the catalytic triad amino acids with the orthosilicic acid (red) modeled in the catalytic pocket of the enzyme. The catalytic triad amino acids Ser26, His165, and Asn185 are marked in blue. The cysteine residues involved in the formation of the three disulfide bridges of silicatein-α are indicated in green. (**b**) Initial step of the catalytic cycle (Heinz C. Schroder et al., 2011)

2. Growth of nuclei and formation of spherical particles (oligomerization).

After hydrolysis of silicon alkoxide to yield silica hydroxide follows the condensation of hydroxyl groups with one another to form the metal oxide network. It happens either through the condensation between two silicon hydroxide species to release water (oxolation) or between a silicon hydroxide and silicon alkoxide to release alcohol (alcoxolation). This step is characterized by collision between ionized and unionized silicic acid molecules. Firstly the monomer oligomerises to form disilicic acid (fig. 3.7) and then forms trimeric, tetrameric, etc. species.

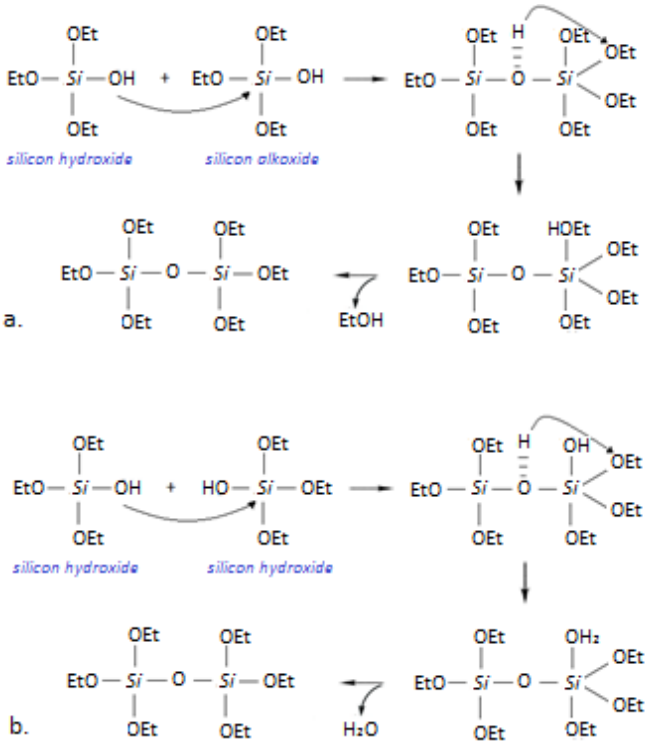

Fig. 3.7 Alcoxolation (a) and oxolation (b) mechanisms. The nucleophilic attack (SN^2 reaction) of the partially negatively charged oxygen of the OH ligand of the silicon hydroxide at the partially positively charged silicon of the a. silicon alcoxide or b. silicon hydroxide results in the formation of a pentavalent intermediate. Subsequently, after a proton transfer, an a. ethanol or b. water molecule is released from the intermediate (Perry and Keeling-Tucker 2000).

3. Aggregation/fusion of particles & Ostwald ripening

Once oligomers dominate, smaller condensation units (monomers, dimmers etc.) react preferentially with them increasing their size. This is due to the higher density of siloxane groups in oligomers which makes them more acidic thus more highly ionized (silanol groups, $Si(OH)_4$, have basic pKa 9.8, in contrast to silica nanospheres which decreases to 6.8). The pka value for the silanol groups (orthosilicic acid, pka 9.8; (Iler 1980)) decreases during the condensation reaction, resulting in a negative charge of the formed silica particles (Perry and Keeling-Tucker 2000). This means that some positively charged molecules or ions are required to neutralize the negative charge on the surface of these particles to allow their aggregation/fusion. Also, larger particles grow through Ostwald ripening (smaller particles, which are more soluble, dissolve and release silicic acid which redeposits onto the surface of the larger particles).

3.3 Synthetic analogues of silicatein

Biologically inspired synthetic analogues of silicatein that are less complex and easier to produce are necessary in order to advance the nanofabrication techniques for potential mass production. The detailed examination of silicatein made it possible to transfer its simplified catalytic mechanism into fundamental design principles that can be translated into synthetic systems. Until now the following synthetic analogues were described that are simple, less expensive, thermally robust and can mimic silicatein:

Bifunctional Block Copolymers

Cha et al. synthesized diblock copolypeptides and examined their catalytic activity at neutral pH. Firstly, he used a (2,2′-bipyridyl)Ni(1,5-cyclooctadiene) initiator for the ring opening polymerization of amino acid *N*-carboxyanhydrides (Cha, Shimizu et al. 1999). The product was a diblock copolypeptide which was further modified with the addition of nucleophile residues (Ser or Cys) at the amine-terminated residues (eg. Lys). After its reaction with TEOS at pH 7 Cha confirmed that:

1. The hydrogen bond between nitrogen groups and Ser (or Cys) residue rendered it more nucleophile for TEOS hydrolysis and
2. The catalytic activity increases with the strength of the nucleophile (Cys>Ser).

The ability of these copolypeptides to self-assemble in different conditions was examined too. In nitrogen atmosphere, they organized into monodisperse spherical aggregates (60nm diameter), while upon their exposure in air, the previously free thiol groups oxidized and formed disulphide bonds, which resulted in fiber structures. Spherical and fiber copolypeptides reacted with TEOS and formed silica coated spheres and fibrillar bundles.

Another attempt to mimic Silicatein's catalytic mechanism was by Adamson et al. (fig. 3.8) (Adamson, Dabbs et al. 2007) who synthesized the diblock copolymer poly(hydroxylated butadiene-*b*-2-vinylpyridine). After the addition of TEOS in pH 7 the nitrogen-containing pyridyl attracted the hydrogen from the hydroxylated butadiene and made it a stronger nucleophile, resulting in silica catalysis. A remarkable difference in the rate of reaction between this polymer and Cha's poly(serine-b-lysine) confirmed that the closer the pKa of nitrogen containing group is to buffers pH, the slower the rate of reaction is.

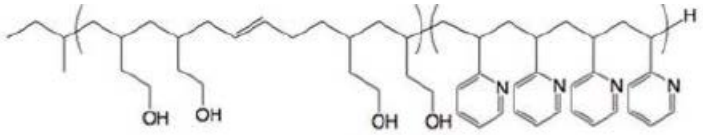

Fig. 3.8 poly(hydroxylated butadiene-*b*-2-vinylpyridine) diblock copolymer synthesized by Adamson et al.

Bifunctional gold surfaces

Kisailus et al. grafted two different populations of gold nanoparticles with the necessary nucleophilic (hydroxyl containing group) and hydrogen bond acceptor (imidazole containing group), which self-organized in monolayers of ω-functionalized organic thiols (fig. 3.9) (Kisailus, Choi et al. 2005). When these two gold nanoparticles approached each other in a distance of 2-3Å (similar to the 2Å hydrogen bonding distance between Ser and His in silicatein protein), a catalytic center was created for TEOS hydrolysis. The result was a formation of a silica network around the gold nanoparticles (fig. 3.10).

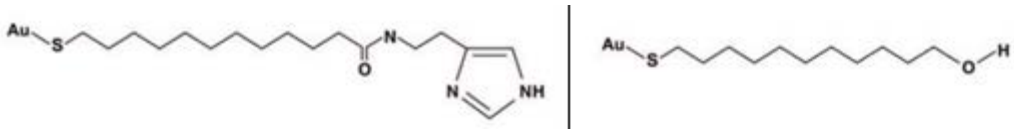

Fig. 3.9 Grafted gold nanoparticles with imidazole and hydroxyl groups, synthesized by Kisailus et al.

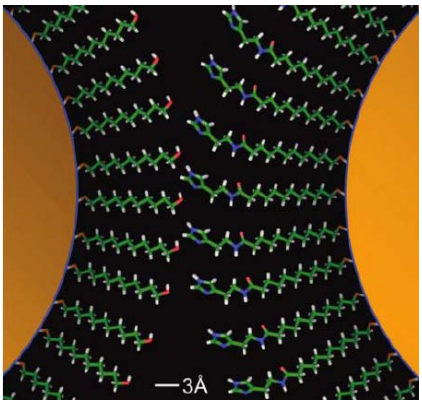

Fig. 3.10 Interaction between two grafted gold nanoparticles (Kisailus et al.)

Small molecule catalysts

Roth et al. examined the ability of small bifunctional molecules to catalyze TEOS hydrolysis by studying cysteamine, ethanolamine, 2-(dimethylamino)ethanethiol hydrochloride (DMAET) and 2-(ethylthio)ethylamine hydrochloride (ETEA) (fig. 3.11) (Roth, Zhou et al.

2005). After their reaction with TEOS all of them formed 40-100nm silica nanospheres, but in different catalytic rates:

Cysteamine was the molecule with the faster catalytic activity followed by ethanolamine. This result argues with previous studies which claimed that Cys is a stronger nucleophile than Ser. ETEA was the third molecule in catalytic rates, due to the reduced nucleophilicity of thioether compaired to the sulfur atom of Cysteamine. Finally, DMAET presented the slower catalysis of TEOS due to the low hydrogen accepting ability of the tertiary amine.

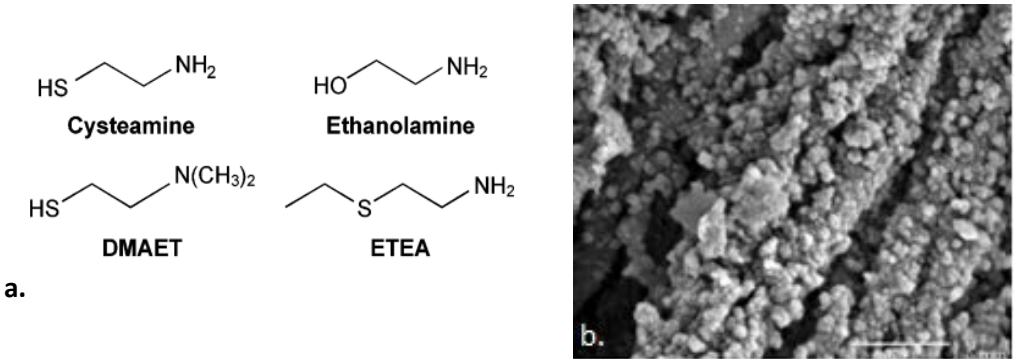

Fig. 3.11 a. Small molecule catalysts synthesized by Roth et al., b. Scanning electron micrograph of silica obtained from the catalytic hydrolysis and polycondensation of TEOS by cysteamine (Roth, Zhou et al. 2005).

3.4 Self-assembling peptides as templates for silica formation

Another organic system that has been used for silica formation and deposition is self-assembling amyloid-like peptides. Pochan and Schneider used the polypeptide MAX8 (fig. 3.12) which could form a fibrillar hydrogel and examined its interaction with silica. The positively charged Lysines of the fibril surface interacted with the negatively charged silica particles and created a uniform silica layer upon them (fig. 3.13) (Altunbas, Sharma et al.).

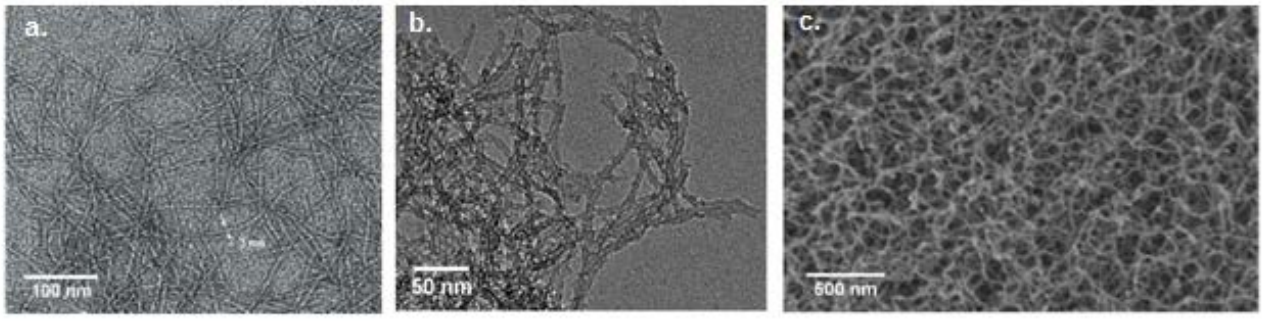

Fig. 3.12 Transmission electron microscopy images of a. negatively stained MAX8 fibrils and b. silica-coated MAX8 peptide fibrils, c. Cryo-SEM image silicified MAX8 fibrils (Altunbas, Sharma et al.).

Aggeli et al. synthesized the peptide CH3CO-Gln-Gln-Arg-Phe-Gln-Trp-Gln-Phe-Glu-Gln-GIn-NH2, which self-assembles into amyloid-like fibrils. The positively charged Arg interacts electrostatically with the negatively charged silica precursor resulting to a silica coated structure (fig. 3.13) (Meegan, Aggeli et al. 2004).

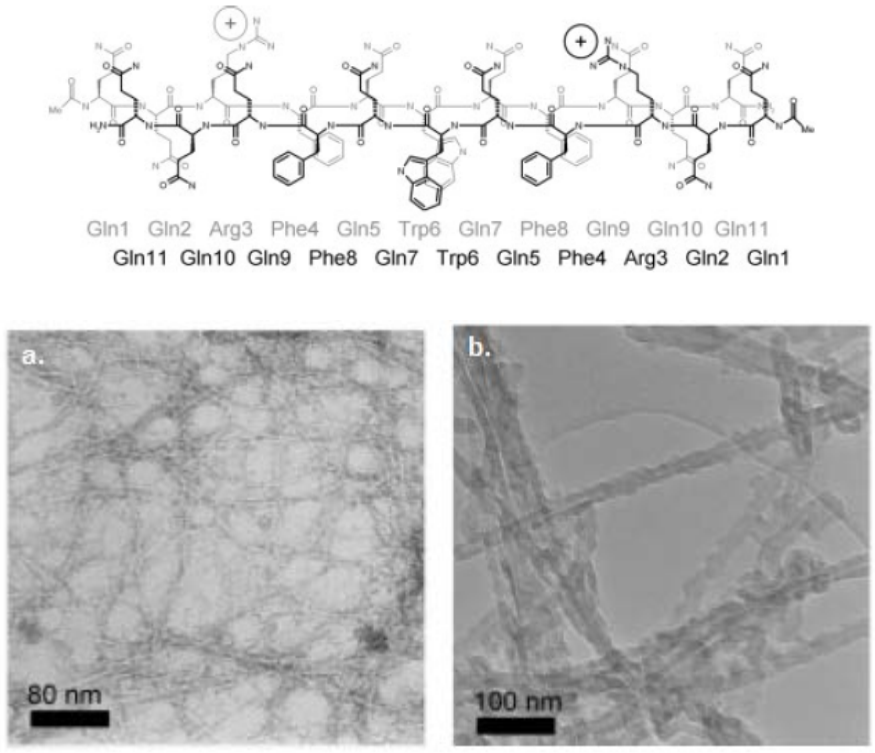

Fig. 3.13 (up) Anti-parallel β-sheet tapes of the synthesized peptide sequence, (down) transmission electron microscopy images of a. negatively stained fibrils and b. silica-coated fibrils (by (Altunbas, Sharma et al.).

Shengjie Wang et al. synthesized the tetra-peptide I3K (three Ile and one Lys residues) which could self-assemble into nanotubes in an aqueous solution. The surface of I3K nanotubes is rich in positively charged lysine residues and therefore provides catalytic sites for the reaction of TEOS (fig. 3.14). The experiment was performed in different solution conditions:

- under weak acidic and neutral pH, where the silica deposition was along the exterior surface of the nanotubes. Because of the low degree of deprotonation of silanol groups, resulting in relatively weak interactions with positively charged Lys.
- over mild basic pH ranges the silica intermediates were highly charged resulting to their deposition along the interior surface of nanotubes too. Initially, silicon species

start to grow on the exterior surface of the nanotubes, however when a saturated thickness is reached the move inside the tube. (Wang, Ge et al. 2011).

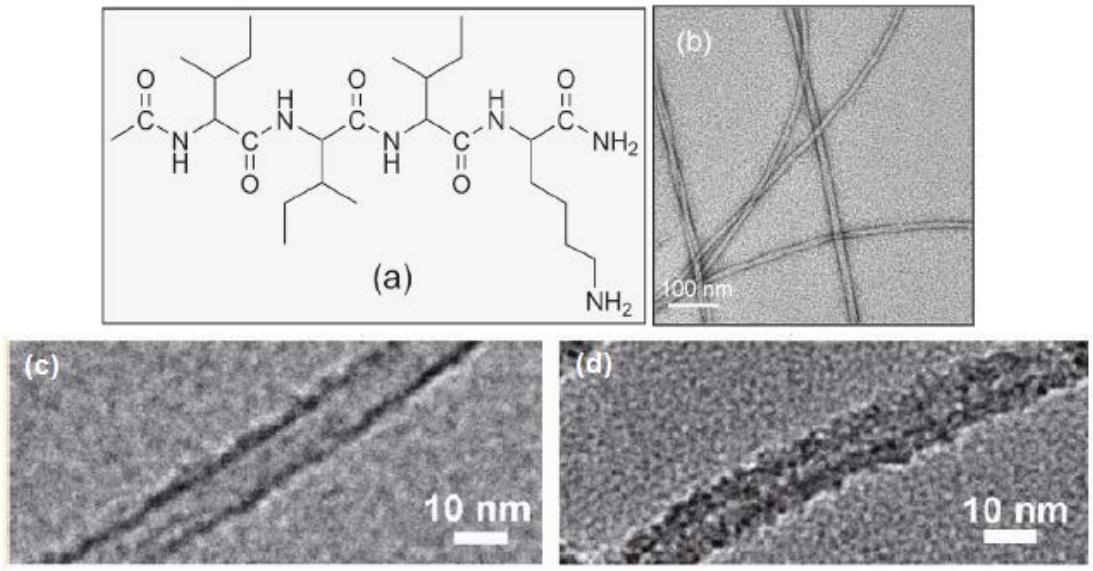

Fig. 3.14 (a) Chemical structure of I3K, (b) negative-stain TEM micrograph showing a nanotubular structure. (c) silica deposition on the outer surface and (d) silica deposition on the inner and outer surface (Wang, Ge et al. 2011).

CHAPTER 4 Thesis rationale

In a previous study of silicatein synthetic analogues in our lab, Kasotakis et al. focused on the ability of the octapeptide NSGAITIG to template silica (Kasotakis, Mossou et al. 2009). The building block NSGAITIG-$CONH_2$ self-assembles into amyloid-like fibers creating a scaffold whose functionality depends on the properties of exposed residues (fig. 4.1). Molecular Dynamics Simulations showed that the part of the peptide responsible for the beta amyloid core is due to the AITI hydrophobic moiety, which adopts a beta-strand conformation, while the NS part remains out of the fibril core forming a type-2 turn (Tamamis, Kasotakis et al. 2009). The role of Ser residue in the silification and templating mechanism was investigated in pH 8, where the N-terminal amino group is uncharged. The pK of the N-terminal group of the peptide was determined to be 6.5 by titration, see below. This pH was chosen in order to have the N-terminal group completely uncharged, and therefore avoid contributions to silica templating by positively charged groups. The key for the beginning of the hydrolysis mechanism is the hydrogen bond formed between the a-amino group of Asparagine and Serine. Subsequently, Serine's oxygen becomes more nucleophilic and attacks the silicon atom (fig. 4.2).

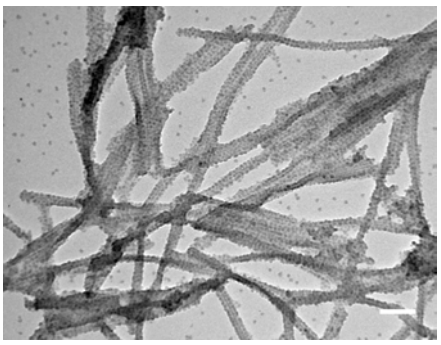

Fig. 4.1 Peptide fibrils after in vitro silification for 15h. The NSGAITIG peptide fibrils nucleate the formation of silica particles on their surface (Scale bar: 100nm) (Kasotakis et al., 2012).

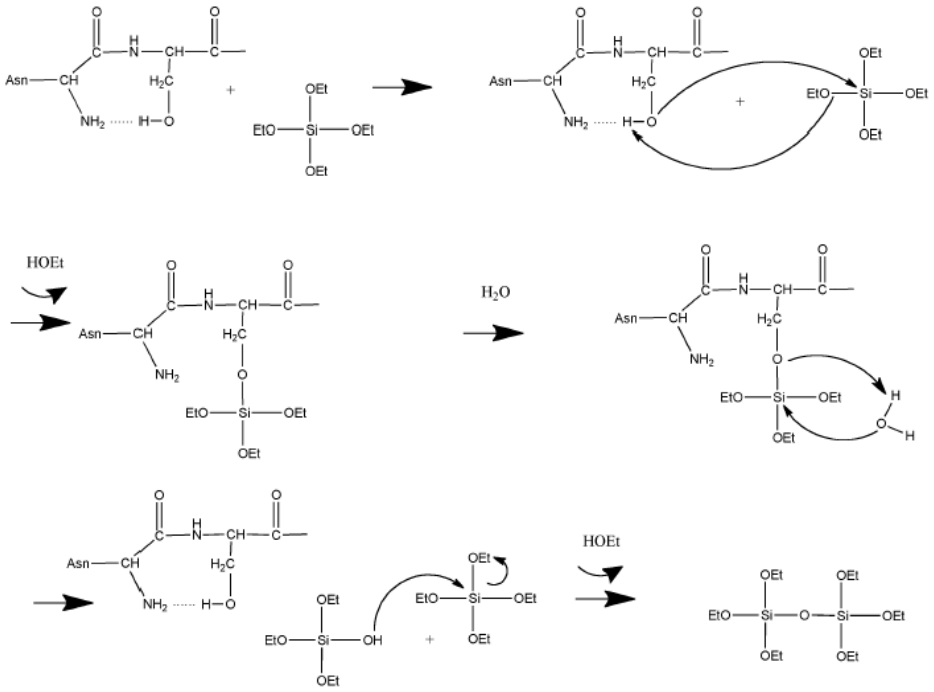

Fig. 4.2 Proposed catalytic mechanism of TEOS from the self-assembling Ac-NH-HSGAITIG-$CONH_2$ peptide (Kasotakis et al.). (Kasotakis, Mossou et al. 2009)

In the present thesis we will move one step forward and prove that the serine residue can be rendered nucleophilic by the amino-containing side group of its adjacent amino acid. This side group will serve as a base in order to attack serine's oxygen and start the TEOS hydrolysis. For this we chose the octapeptide Ac-NH-HSGAITIG-$CONH_2$ which in comparison to NSGAITIG-$CONH_2$ differs only by the first amino acid and the acetylated N-terminal amino group. We presumed that Ac-NH-HSGAITIG-$CONH_2$ will adopt the same conformation expecting similar silica template nanofibers, thus the only responsible amino acids for its hydrolytic and templating character will be His and Ser. In order to test this hypothesis we chose as control peptides the octapeptides:

- Ac-NH-HAGAITIG-$CONH_2$ where there is lack of Ser, in order to test whether the hydroxyl group of serine is necessary for attacking the silicon substrate and hydrolyse it and
- Ac-NH-ASGAITIG-$CONH_2$ where there is lack of His, in order to test if His is essential due to its basic ability to set the oxygen of hydroxyl Ser residue a better nucleophile (fig. 4.3).

Ac-NH-**HS**GAITIG-$CONH_2$

Acetyl- His - Ser - Gly - Ala - Ile - Thr - Ile - Gly – Amide

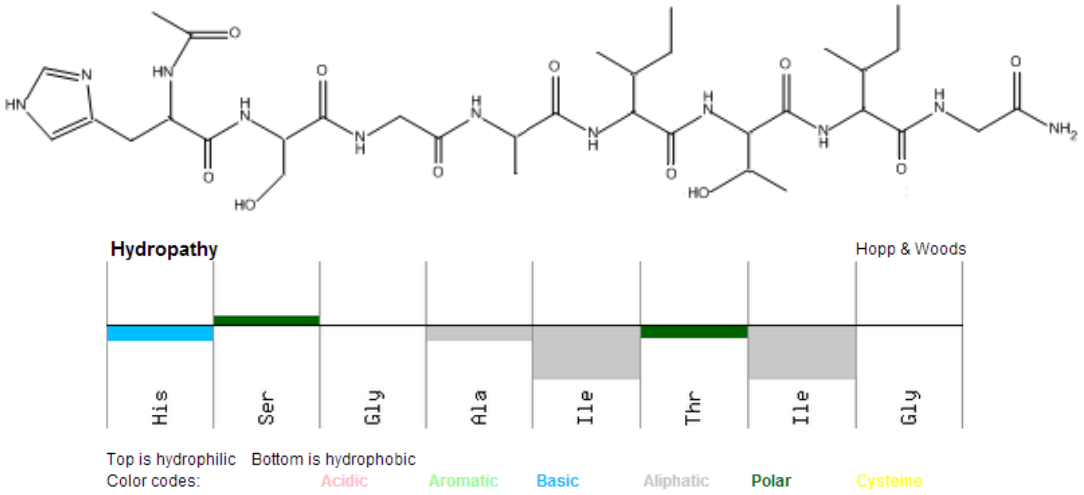

Ac-NH-**HA**GAITIG-$CONH_2$

Acetyl- His - Ala - Gly - Ala - Ile - Thr - Ile - Gly –Amide

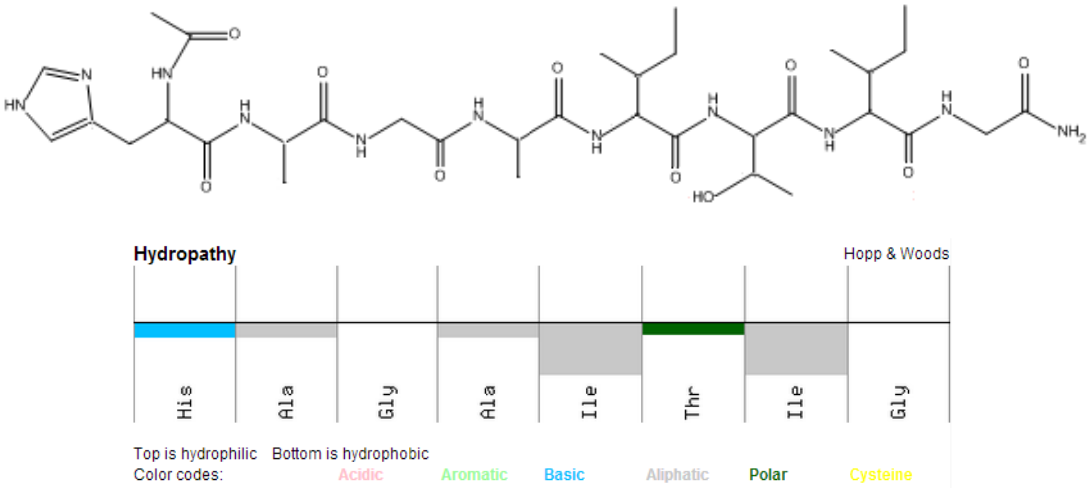

Ac-NH-**AS**GAITIG-$CONH_2$

Acetyl- Ala - Ser - Gly - Ala - Ile - Thr - Ile - Gly –Amide

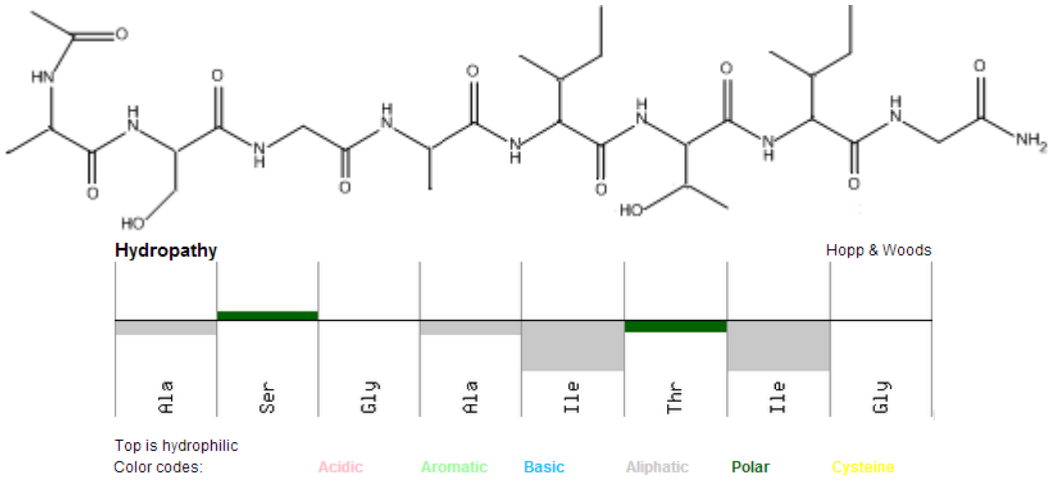

Fig. 4.3 Selected peptide building blocks for in vitro silicification.

CHAPTER 5 Experimental Techniques

5.1 Transmission electron microscopy (TEM)

The experiments of Transmission Electron Microscopy (TEM) were performed in the Department of Biology University of Crete, using a JEOL JEM-100C microscope operating at 80kV. In TEM, a cathode ray source is used to emit and accelerate a high-voltage electron beam, which is focused and guided by electromagnetic lenses. When the electrons pass through the thin and electron-transparent specimen, an image is formed, magnified and focused again by objective lenses in order to appear again in a two dimensional picture on a fluorescent screen.

5.2 Field-emission scanning electron microscopy (FESEM)

The experiments of FESEM were performed at the Department of Biology of the University. FESEM is used to visualize very small topographic details on the surface of objects as small as 1 nanometer. In a FESEM electrons are emitted from a source and accelerated in a high electrical field gradient. These primary electrons are focused and deflected by electronic lenses to produce a narrow scan beam that bombards the object. The scattered electrons are collected by a detector and after they pass through an electronic signal amplification and digitalization, a three-dimensional shadow-cased image appears in the computer screen. In order to prevent charging of the specimen during its interaction with the electron beam, we cover it with a thin layer of conducting material, such as 10nm of gold, through a process called sputtering.

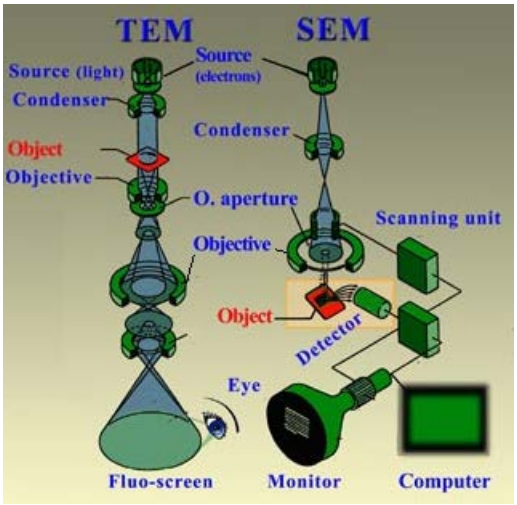

Fig. 5.1 Transmission and Field-Emission electron microscopes.

5.3. Critical point drying (CPD)

Evaporation in specimens damages the microscope during their examination and distorts their surface structure due to effects of high surface tension. Thus the specimen medium, which is water in biological structures, has to be replaced with another liquid of a minimum surface tension. Such a liquid is CO_2, whose critical point of liquid and vapor phase coexistence corresponds to a temperature of 35°C and pressure of 1200 psi. CPD relies in that critical phenomenon, where temperature is raised upon CO_2 critical point resulting to its transition into vapor without any surface tension effects. Finally, in this procedure another intermediate liquid is involved, such as ethanol, which allows the sufficient mixture of CO_2 with water.

5.4 Raman spectroscopy

The experiments of Raman spectroscopy performed in the IESL-FORTH institute in Heraklion, Crete. Raman spectroscopy is used to observe the structural characteristics of a sample due to the vibrational, rotational, and other low-frequency modes of the molecular bonds. When the laser light of a spectroscope interacts with the free electron gas and molecular bonds of a sample it causes their excitation from a ground state to a higher one. The scattering of electrons and modes which return to their initial state is called Rayleigh. However, if they return to another state there is an energetic difference which results to a photon emission. This inelastic scattering, because of the energy transfer is called Raman scattering, which is distinguished into Stokes and anti-Stokes. In Stokes the final vibrational state of the molecule has higher energy than its ground state, while in anti-Stokes the energetic difference is smaller (fig. 5.2). These scattering shifts are measured and give information about the rotational and vibrational states of the sample.

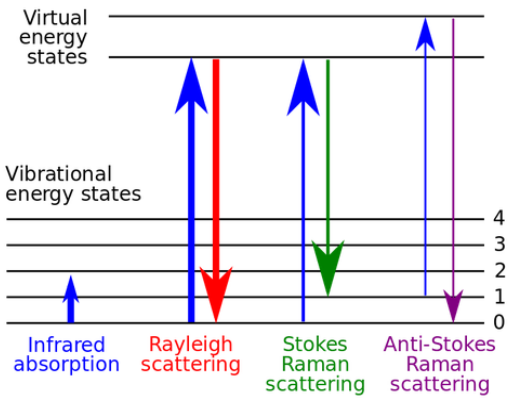

Fig. 5.2 Energy level diagram depicting Rayleigh and Raman scattering. The line thickness is roughly proportional to the signal strength from the different transition.

The peptide group, gives up to 9 characteristic bands named amide A, B, I, II ... VII. Each one has a characteristic absorption band which depends on specific vibrations (table 5.1).

Designation	Approximate Frequency (cm^{-1})	Description
Amide A	3300	NH stretching
Amide B	3100	NH stretching
Amide I	1600-1690	C=O stretching
Amide II	1480-1575	CN stretching, NH bending
Amide III	1229-1301	CN stretching, NH bending
Amide IV	625-767	OCN bending
Amide V	640-800	Out-of-plane NH bending
Amide VI	537-606	Out-of-plane C=O bending
Amide VII	200	Skeletal torsion

Table 5.1 Amide bands and their characteristic vibrations (http://www.biocompare.com/Application-Notes/118761-The-Direct-Detect-Biomolecular-Quantitation-System/)

5.5 Titration

Since amino acids, and therefore peptides, incorporate acidic and basic functional groups, the predominant molecular species present in an aqueous solution will depend on the pH of the solution. In order to determine the surface properties of a peptide and its behavior in aqueous solutions at different pH's, we make use of the Henderson - Hasselbalch Equation:

$$pK_a = pH + \frac{\log[HA]}{[A^-]}$$

pK_a represents the acidity of a specific conjugate acid function (HA). An experimental demonstration of the above equation is given by a titration curve where the pH changes in a characteristic way. Titration describes a chemical reaction between two solutions by the controlled addition of one solution (titrant) to the other. The titration curve that originates is a graph of the pH as a function of the amount of titrant (acid or base) added. A characteristic acid-base titration curve is demonstrated in fig. 5.3 were the buffer regions, number and pKa of ionizing group(s) are shown.

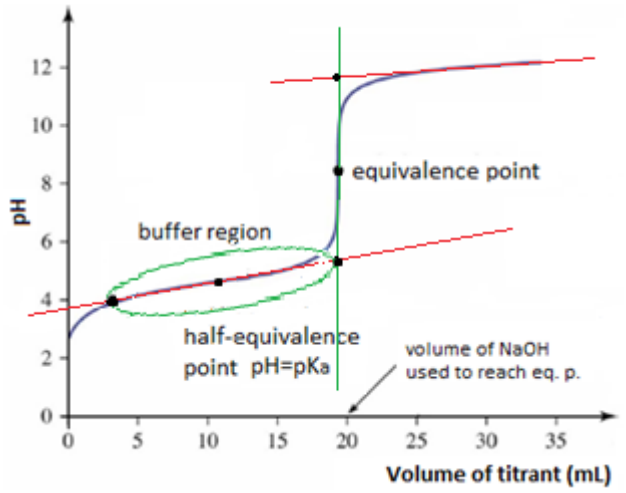

Fig. 5.3 Acid-base titration curve and its characteristics.

For a weak acid/strong base titration curve there are four points of interest:

1. Initial point. It indicated the pH of the titrated solution (weak acid) before its reaction with the titrant. $pH = -\log[acid]$.
2. Buffer/acid region. In this region there is a small change in pH due to the relatively small changes in H^+ concentration. At the center of buffer region there is the half-equivalence point (midpoint), whose pH equals to the log of the ionization constant (pKa) of the acid. Up to this point the half of the acid concentration has been titrated. $pH = pKa = -\log\left[\frac{\textbf{moles acid} - \textbf{moles base}}{\textbf{Vol acid} + \textbf{Vol base}}\right]$ (eq. 1) (the acid is the one that did not react).
3. Equivalence point. Around this point, relatively small changes in H^+ concentration cause large changes in pH. The center of the vertical region is the equivalence point, where the acid solution becomes neutral Moles of base=moles of acid.
4. Strong base region. In this region OH^- dominates

$$pH = 14 - p[base] = 14 - log\left[\frac{moles\ base - moles\ acid}{Vol\ acid + Vol\ base}\right]$$

There are two methods to locate the equivalence and half-equivalence point in a titration curve:

A. Geometric method: We draw two lines each of one follows the most horizontial part of buffer and strong base region and a line that follows the most vertical part of the curve. The geometric center in the distance between the top and bottom intersection is the equivalence point and its x-coordinate equals to the volume of the equivalence point.

The half distance between the starting point of the curve and the bottom intersection is the midpoint, while its y-coordinate equals to the pKa of the acid.

B. Derivative method: We calculate the first derivatives: $\frac{dpH}{d\left(vol\ base/vol\ acid\right)}$ and $\frac{d\left(vol\ base/vol\ acid\right)}{dpH}$. The peak in each graph indicates the equivalence and half-equivalence point respectively.

The peptide titration experiment was performed in the “Biology and Technology” institute in Saclay, Paris by Dr. Kasotakis Manolis.

CHAPTER 6 Methodology

6.1 Peptide self-assembly

Lyophilized peptide powders with a degree of purity higher than 95% were purchased from Eurogentec (Belgium). Peptides were dissolved in Tris-HCl buffer (pH 8 & 6.8, c=25 mM) at concentration 2 mg/ml.

6.2 In vitro silification protocol

After 24h of peptide self-assembly we added tetraethyl orthosilicate ($Si(OC_2H_5)_4$, TEOS) precursor in a 5:3 volume ratio (for 500µl of Buffer we added 300µl TEOS). A very critical point in Si hydrolysis and template was the gentle addition of TEOS without mixing it with the peptide gel. At the same time a control solution of buffer and TEOS (ratio 5:3) was prepared without peptides. A biphasic solution was formed and the silification took place under gentle shaking (150 rpm) for 8 days.

6.3 Sample preparation

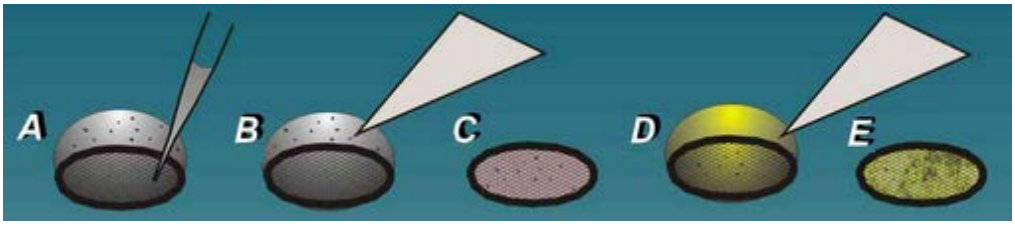

Fig. 6.1 Peptide TEM imaging preparation

After 24h of self-assembly 10 mL of each peptide solution was pipette on to a 300 mesh formvar-coated grid. 2 min after sample's absorption, the droplet was carefully removed with a blotting paper. In order to enhance the contrast of fibers we stained them with 10mL of PTA (1% phosphotungstic acid in water). After 2 min of proper absorption the extra solution was removed. The last step was to allow the grid to air-dry for 24h (fig. 6.1).

B. Si/peptide TEM preparation

10 days after silica polymerization we removed the supernatant, sonicated the samples for 5 seconds in order to release the silica nanoparticles which were trapped in between the fibers, diluted the pellet in distilled water and centrifuged it (for 5 min, 1000 rpm). The supernatant was removed with all non-templated Si particles in order to obtain the template

Si on fibers surface. This process was repeated for three times before samples placement on formvar-coated grid (no negative staining was used).

C. Raman spectroscopy/peptide preparation

In order to examine the secondary structure of fibers we dropped 10 μl of the sample in between two aligned thin glass rods and we left it to dry. After the formation of a thin solid fiber we examined it in Raman spectroscopy (fig. 6.2).

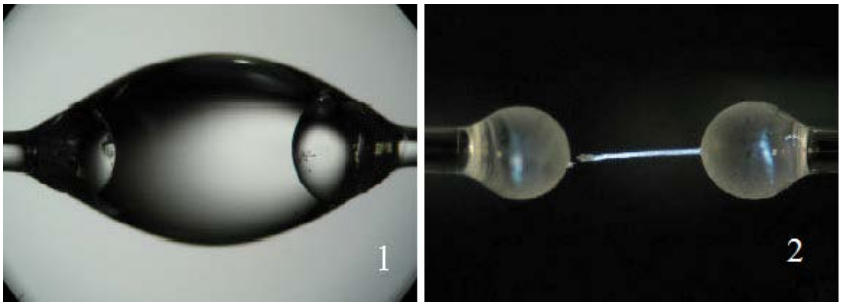

Fig. 6.2 Peptide preparation for Raman spectroscopy: 1) Addition of a 10 μl drop in between two aligned glass rodes and 2) Formation of a thin solid fiber.

D. Field-emission observation of Si/peptides

Samples for field-emission imaging need to be dried because water molecules disturb the vacuum (thus imaging) and can cause massive deformation or collapse of the observed structures. Thus the protocol of critical point drying was applied:

As holder conical beem capcules (size 00) were used, whose bottom was cut-off (a) and replaced by a punched nucleopore track-etch membrane (b). Samples supernatant was removed and the pellet was placed in the holder (c) as seen in fig. 6.3. The remained liquid phase penetrated through filter's pores.

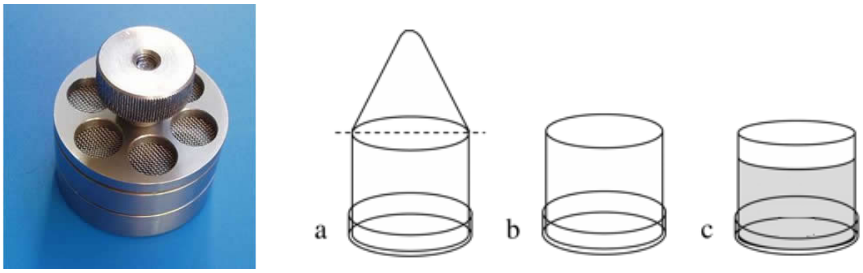

Fig. 6.3 Holder for beem capsules and their preparation (a,b,c).

Then the below steps were followed:

1. Sample washing with SCB for 10 min (x2).
2. Fixation with GDA 2%, PFA 2% in SCB for 30 min in order to increase mechanical and

thermal stability of peptide cross links.

3. Repetition of 1st step.

4. Second fixation with osmium, O_5O_4 , for 30 min.

5. Repetition of 1st step.

6. Gradual dehydration with 30% (10 min), 50% (10 min) and 70% (24 h) ethanol.

7. Extra dehydration with 90% and 100% ethanol (10 min each). In dehydration the ascending concentration of ethanol replaces water molecules minimizing the surface tension effects).

8. Addition of dry-alcohol for 10 min and capping of holder with a nucleopore track-etch membrane, which was placed into the CPD instrument.

6.4 **Titration setup**

For the peptide titration we applied the following protocol:

1. We dissolved $1*10^{-3}$ g of each peptide in 1mL water.
2. Filled a syringe pump (Model 100 Series – KD) with a 0.05M NaOH solution and calibrated it in a rate of 30μL/h.
3. After each addition of titrant measurements were taken from the level of pump and the pH meter.
4. Once the pH started to change more rapidly the rate of NaOH additions was reduced to its half, until the titration came to an end at approximately pH 11.

CHAPTER 7 Experimental results and Discussion

7.1 Titration curves

We applied the previously described analysis methods (see chapter 5) in each titration curve and came to the following conclusions:

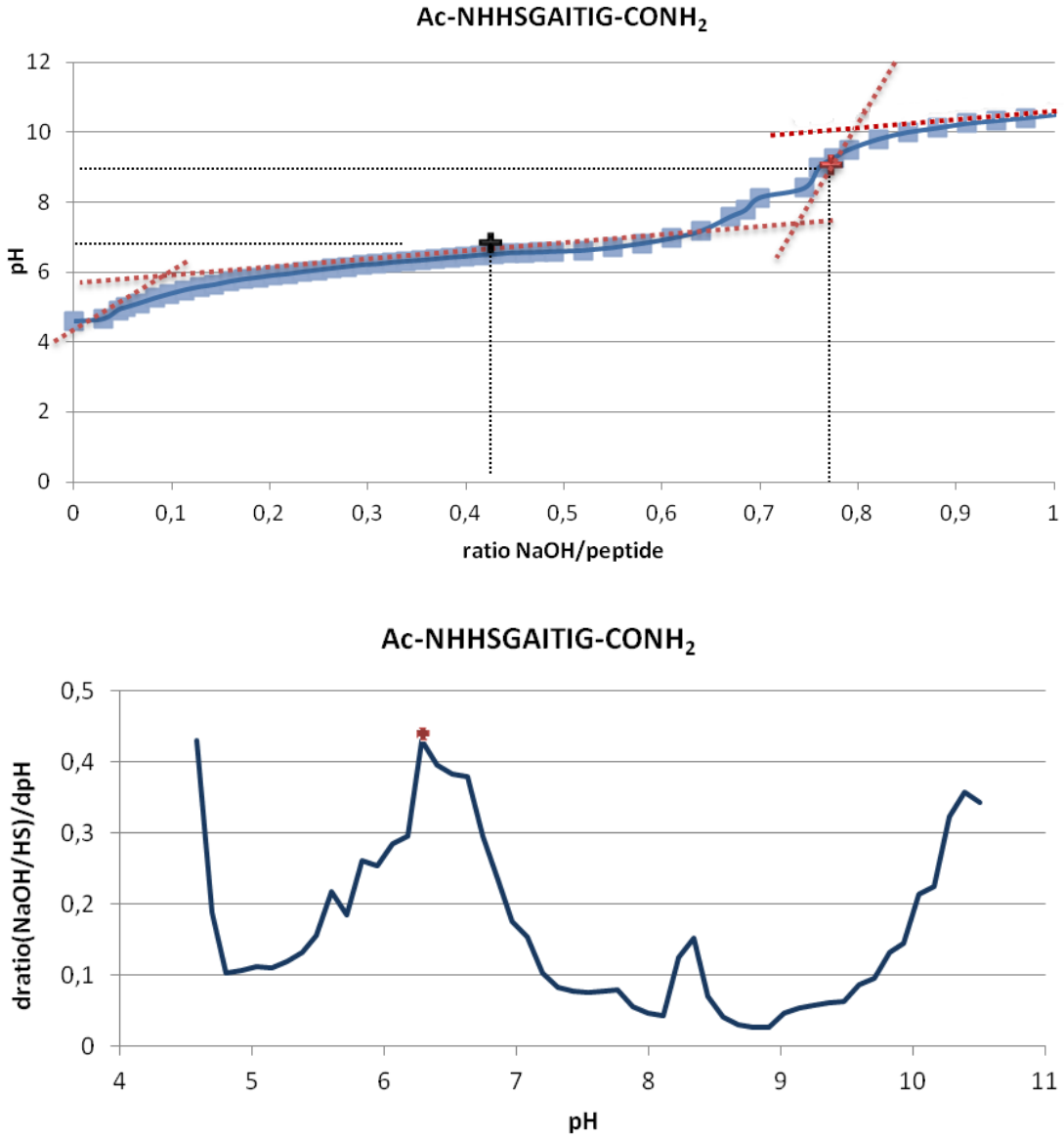

Fig. 7.1 Titration curve of Ac-NH-HSGAITIG-$CONH_2$ peptide (up) and its first derivative $\frac{d\left(vol\ base/vol\ acid\right)}{dpH}$ (bottom).

1. The initial point of Ac-NH-HSGAITIG-$CONH_2$ peptide is at 4.65 pH revealing its weak acidic character. In this point the imidazole group of His is fully protonated, thus the concentration of $[H^+]$ cations is 100%.
2. Buffer region starts from pH=pK-1 and ends at pH=pK+1. In its middle there is located the half equivalence point where pH=pK=6.28. This means that the moles of reacted $[H^+]$ equals to these of $[OH^-]$ and their concentration in the solution is precisely 50%. Taking into account the equation 1 (chapter 5.5) we find that for pH=pK-1=5.28, $[H^+]$=90% and $[OH^-]$=10%, while for pH=pK-1=7.28, $[H^+]$=10% and $[OH^-]$=90%.
3. Equivalence point. As more titrant is added, all of the $[OH^-]$ reacts with $[H^+]$ and the peptide dissociates. As the equivalence point is approached (at pH 8.25) small additions of base cause larger changes in pH and the slope steeps significantly.
4. Base region. Beyond the equivalence point region pH is determined only by the concentration of the excess of NaOH, since there are not any hydrogen cations to react.

Concluding, the peptide Ac-NH-HSGAITIG-$CONH_2$:

1. Have one ionizing group, revealing its monoprotic character.
2. It is weak acid, due to the fact that its dissociation happens in an alkaline region.
3. The first derivative curve confirms our first estimation of half-equivalence point at 6.28.

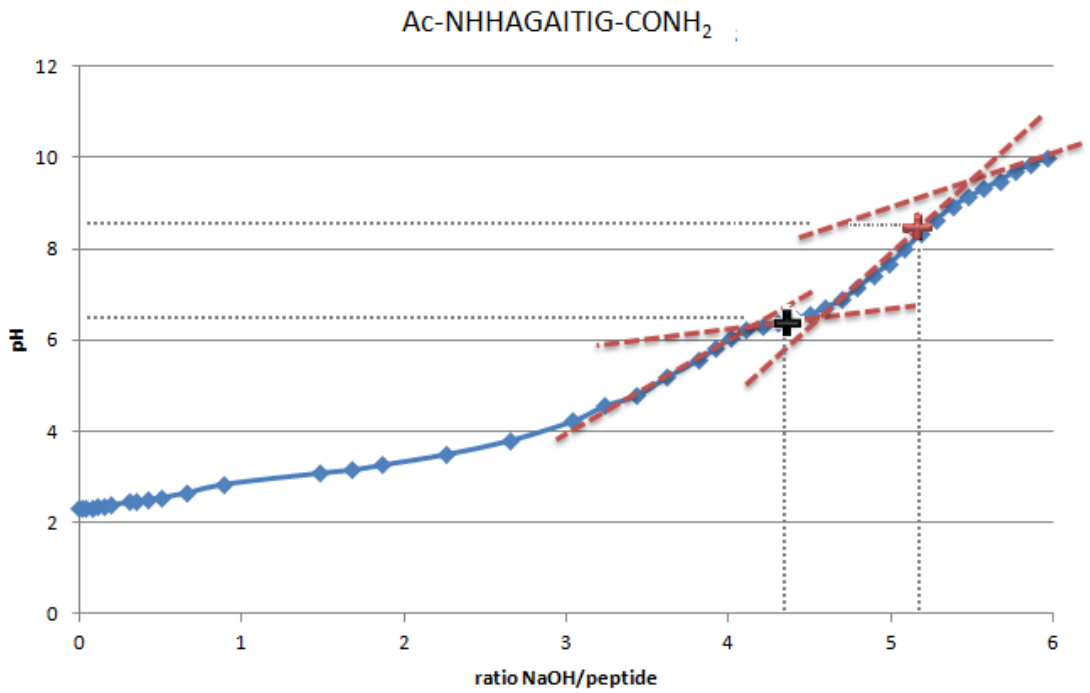

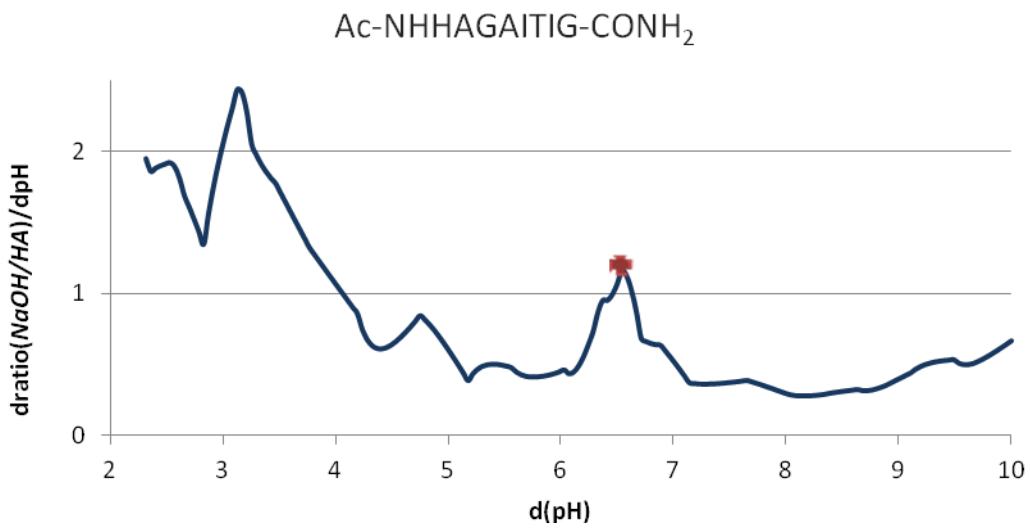

Fig. 7.2 Titration curve of Ac-NH-HAGAITIG-$CONH_2$ peptide (up) and its first derivative $\frac{d\left(^{vol\ base}/_{vol\ acid}\right)}{dpH}$ (bottom).

1. The initial point of Ac-NH-HAGAITIG-$CONH_2$ peptide is at pH 2.31 revealing its weak acidic character. In this point the imidazole group of His is fully protonated, thus the concentration of $[H^+]$ cations is 100%.
2. Buffer region starts from pH=pK-1=5.53 and ends at pH=pK+1=7.53. The half equivalence point is at pH=pK=6.4. This means that the imidazole group neutralizes for pH≥6.28.
3. Equivalence point. Around this part, the curve rises fast, due to the low concentration of hydrogen ions. As more titrant is added, all of the $[OH^-]$ reacts with $[H^+]$ and the peptide dissociates. As the equivalence point is approached (at pH 8) small additions of base cause larger changes in pH and the slope steeps significantly.
4. Base region. Beyond the equivalence point region (or the equivalence point itself?!) pH is determined only by the concentration of the excess of NaOH, since there are not any hydrogen cations to react.

Concluding, the peptide Ac-NH-HAGAITIG-$CONH_2$:

4. Has one ionizing group, revealing its monoprotic character.
5. It is weak acid, due to the fact that its dissociation happens in an alkaline region.
6. The first derivative curve confirms our first estimation of half-equivalence point at pH 6.53.

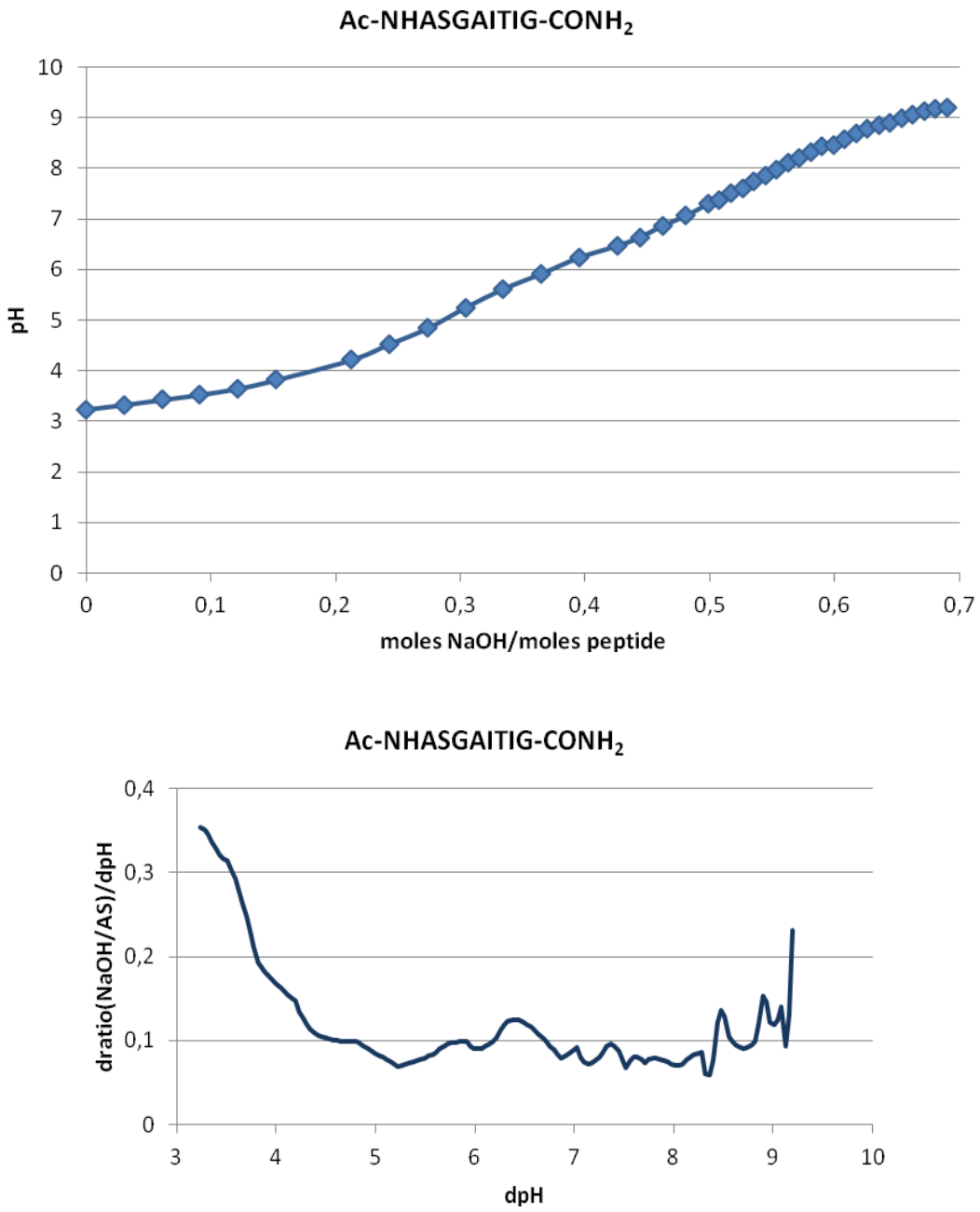

Fig. 7.3 Titration curve of Ac-NH-ASGAITIG-$CONH_2$ peptide (up) and its first derivative $\frac{d\left(vol\ base/vol\ acid\right)}{dpH}$ (bottom).

The peptide Ac-NH-ASGAITIG-$CONH_2$ presents a gradual increase of pH because it lacks ionizing groups on its surface. Also, the first derivative curve shows that there is not an equivalence point. Thus its functionality is not affected by changes of pH.

7.2 Raman spectroscopy

Amide 1 (1600-1690 cm^{-1}, C=O stretching), amide 2 (1480-1575cm^{-1}, CN stretching, NH bending) and amide 3 (1229-1301 cm^{-1}, CN stretching, NH bending) are the three most prominent vibrational bands of the peptide backbone. Generally peaks from 1620-1640 cm^{-1} are assigned to parallel β-sheet conformation, while the band area 1680-1690 cm^{-1} is associated with the presence of antiparallel β-sheet conformation. The following graphs reveal the secondary structure and molecuat vibrations of our peptides.

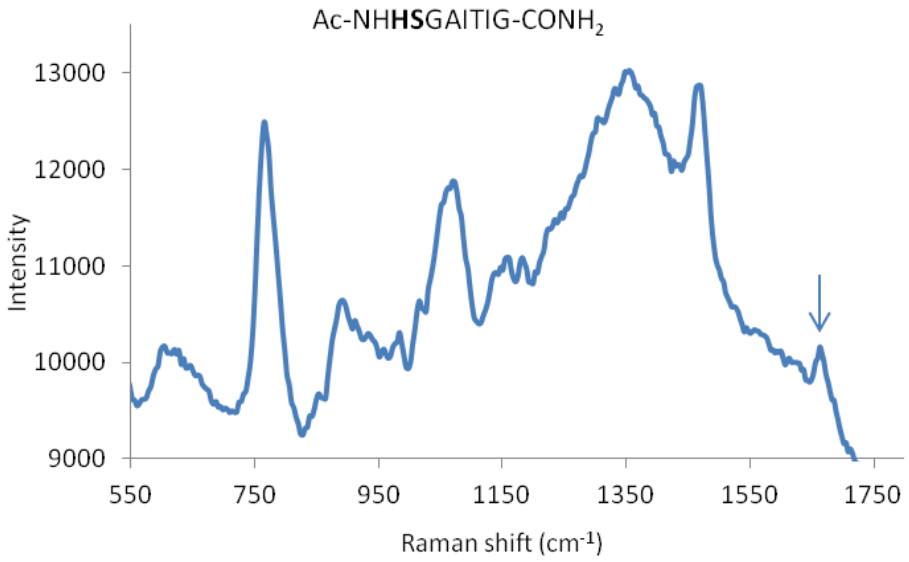

Fig. 7.4 Raman graph of Ac-NH-HSGAITIG-$CONH_2$ peptide.

At the peptide Ac-NH-**HS**GAITIG-$CONH_2$ the absorption at 1655 cm^{-1} belongs to amide 1 region, the following peaks at 1458 and 1343 cm^{-1} are due to Raman spectroscopy.

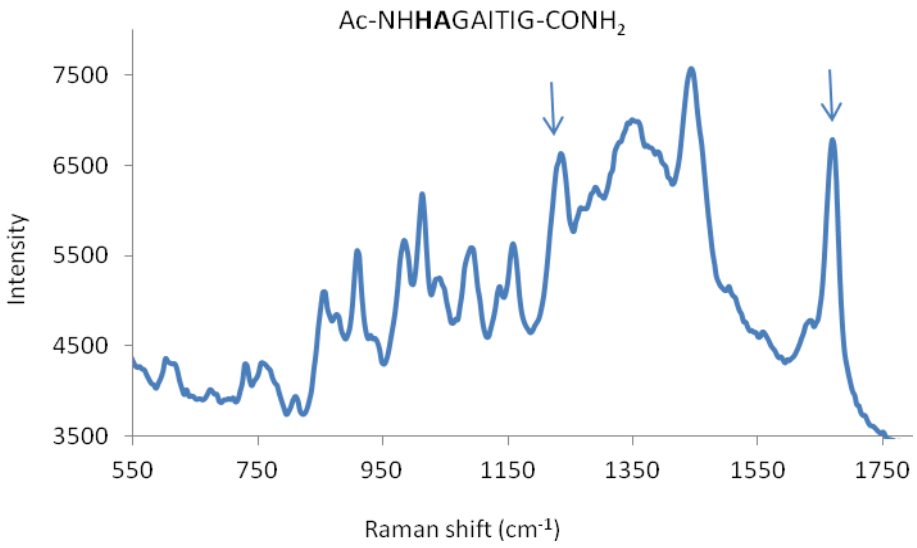

Fig. 7.5 Raman graph of Ac-NH-HAGAITIG-$CONH_2$ peptide.

Ac-NH-**HA**GAITIG-CONH2 presented a characteristic peak at 1668 cm^{-1} which is part of amide 1 region. The peaks at 1435 and 1336 cm^{-1} are due to Raman spectroscopy and the band at 1233 cm^{-1}, describe CN stretching and NH bending (or amide 3 region).

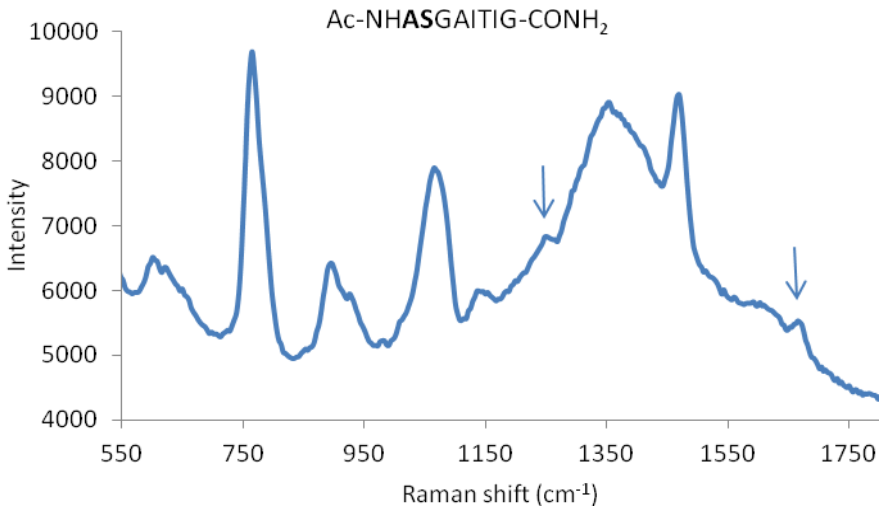

Fig. 7.6 Raman graph of Ac-NH-ASGAITIG-$CONH_2$ peptide.

Ac-NH-**AS**GAITIG-CONH2 displayed a characteristic band at 1664 cm^{-1} which belongs in the amide 1 region. The band at 1246 cm^{-1} belongs to amide 3 region, while the peaks at 1465 and 1343 are due to Raman spectroscopy.

7.3 Peptide self-assembly

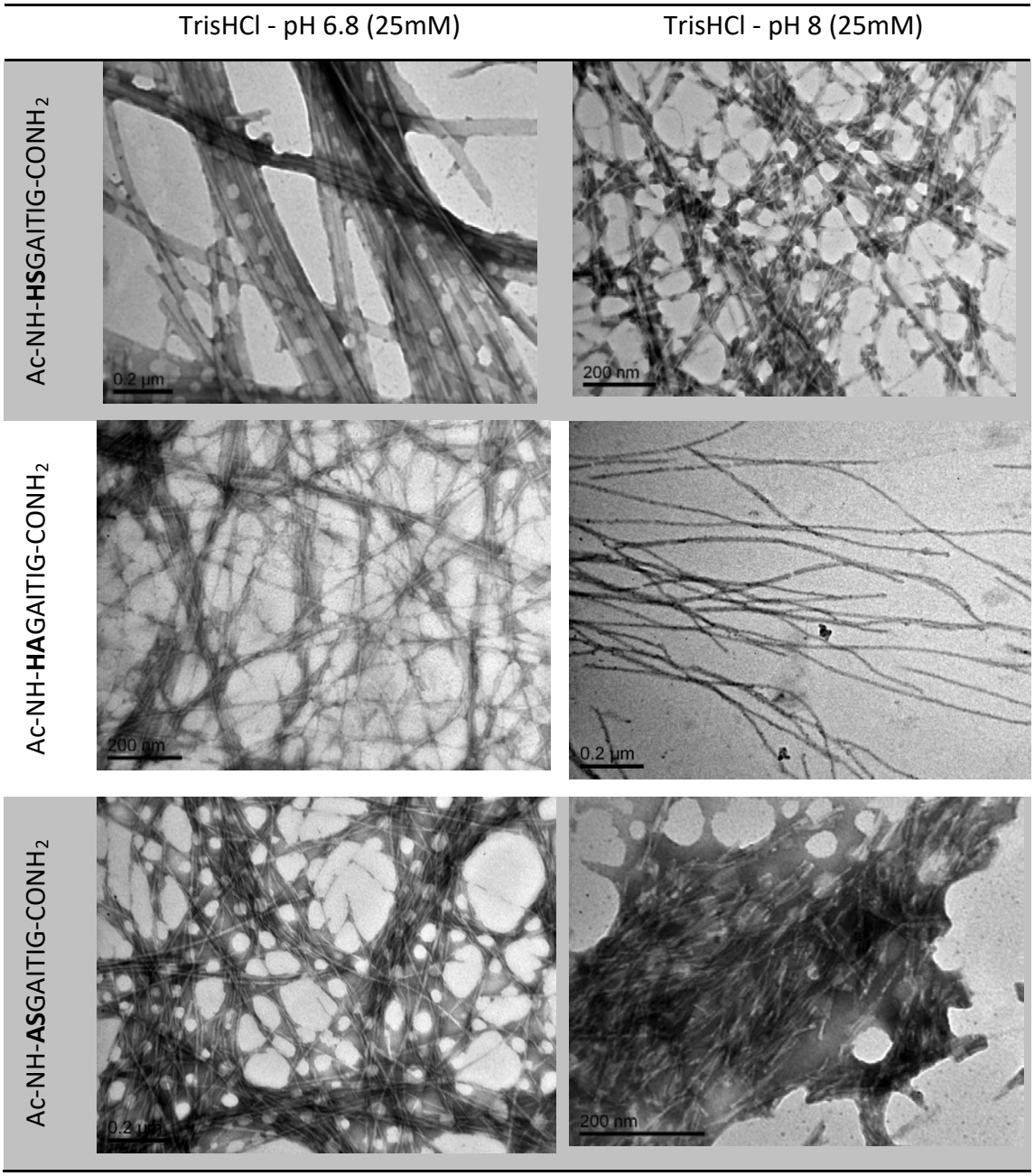

Fig. 7.7 Transmission Electron Microscopy images of the Ac-NH-HSGAITIG-$CONH_2$, Ac-NH-HAGAITIG-$CONH_2$, Ac-NH-ASGAITIG-$CONH_2$ peptide fibrils after 24h of self-assembly in Tris pH 6.8 & 8 (negative staining with PTA).

Transmission Electron Microscopy images show that peptides self-assemble into a fibrillar amyloid-like gel network in TrisHCl buffer of both pH 6.8 and 8. Single fibril diameters and lengths were measured for each peptide. All of them presented the same diameter at 3.84±0.6nm and their length was some microns.

Fig. 7.8 Peptide hydrogels formed from the peptides Ac-NH-HSGAITIG-$CONH_2$, Ac-NH-HAGAITIG-$CONH_2$ and Ac-NH-ASGAITIG-$CONH_2$ (in TrisHCl pH 8) after 24 hours of self-assembly.

7.4 Peptide silicification

After 24h of peptide self-assembly, we followed the silicification protocol and took TEM samples after 24h and 8 days of incubation. We did not use negative staining since the silica nanoparticles provided the necessary contrast.

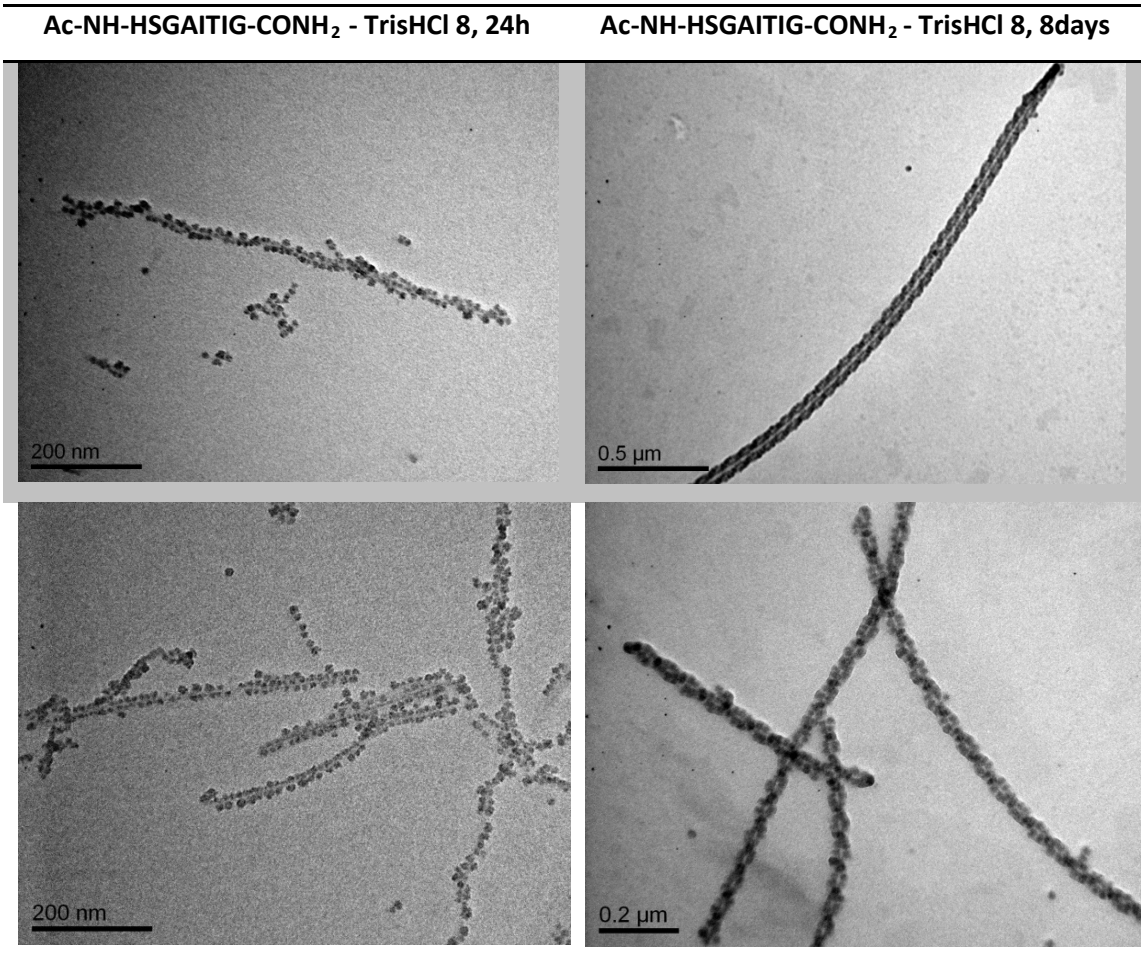

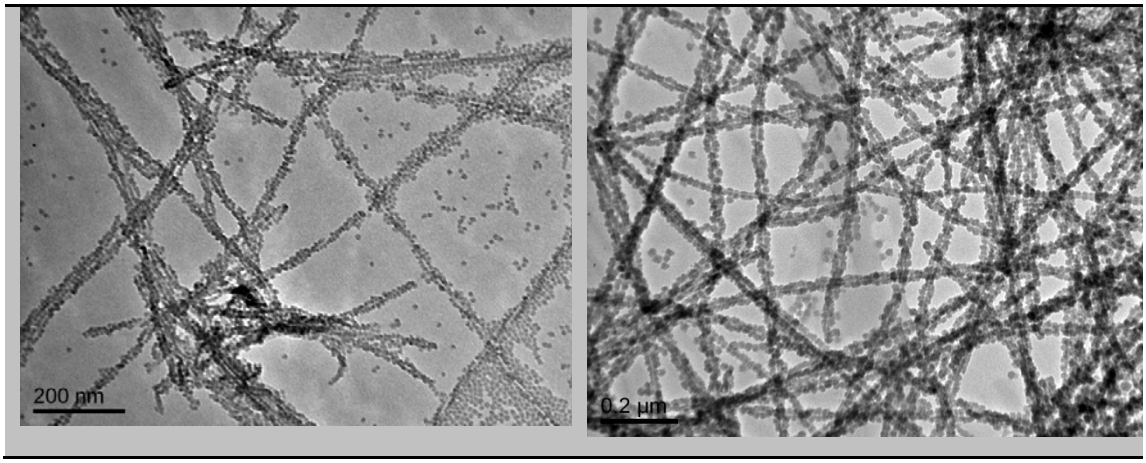

Fig. 7.9 Transmission Electron Microscopy images of the Ac-NH-HSGAITIG-$CONH_2$ peptide fibrils in TrisHCl pH 8 after *in vitro* silicification for 24h (left column) and 8days (right column).

Ac-NH-HSGAITIG-$CONH_2$ (TrisHCl pH 8)

24hours of silicification: Ac-NH-HSGAITIG-$CONH_2$ fibrils were covered by monodispersed silica nanoparticles of d= 10±2nm.

8days if silicification: The solution was washed and new TEM images were taken. The fibrils were templated with silica nanoparticles of d= 17.9±2nm. Their regular deposition revealed the twisting nature of fibrils (pitch=227±3nm). Finally, the number of free silica nanoparticles was negligible.

Ac-NH-HAGAITIG-$CONH_2$ - TrisHCl 8 - 24h	Ac-NH-HAGAITIG-$CONH_2$ - TrisHCl 8 - 8days

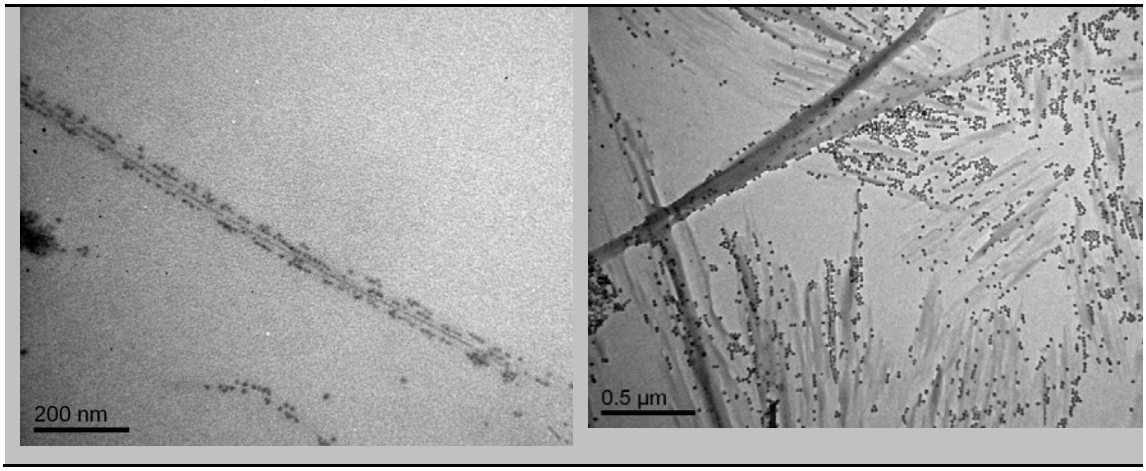

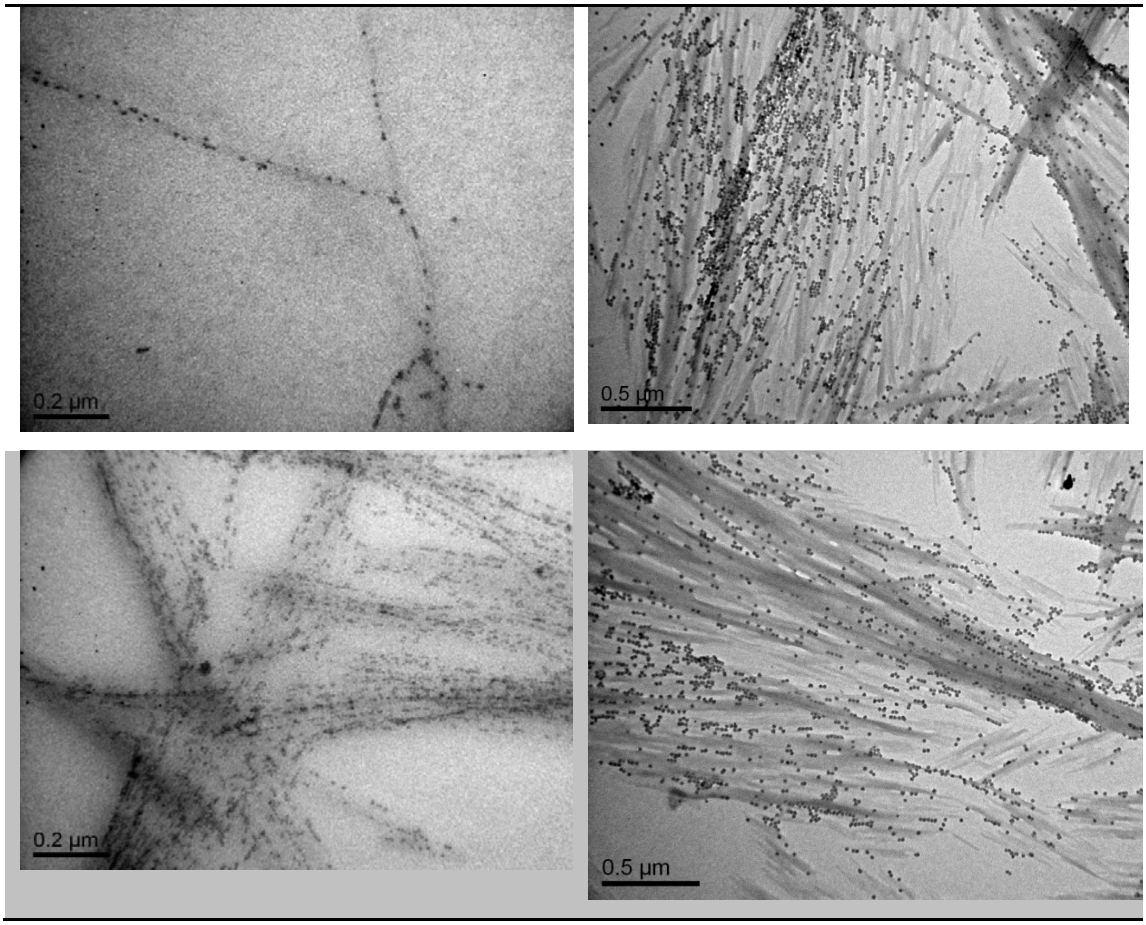

Fig. 7.10 Transmission Electron Microscopy images of the Ac-NH-HAGAITIG-$CONH_2$ peptide fibrils in TrisHCl pH 8 after *in vitro* silicification for 24h (left column) and 8days (right column).

Ac-NH-HAGAITIG-$CONH_2$ (TrisHCl pH 8)

24 hours of silicification: Ac-NH-HAGAITIG-$CONH_2$ images showed fibrils coexisting with silica nanoparticles of a d= 9±1 nm. There is not any regular template upon their surface.

8 days of incubation: Upon washing, there were still observed some silica nanoparticles of d=14±3 nm. This is probably due to the high viscosity of Ac-NH-HAGAITIG-$CONH_2$ hydrogel, which traps silica particles in its network.

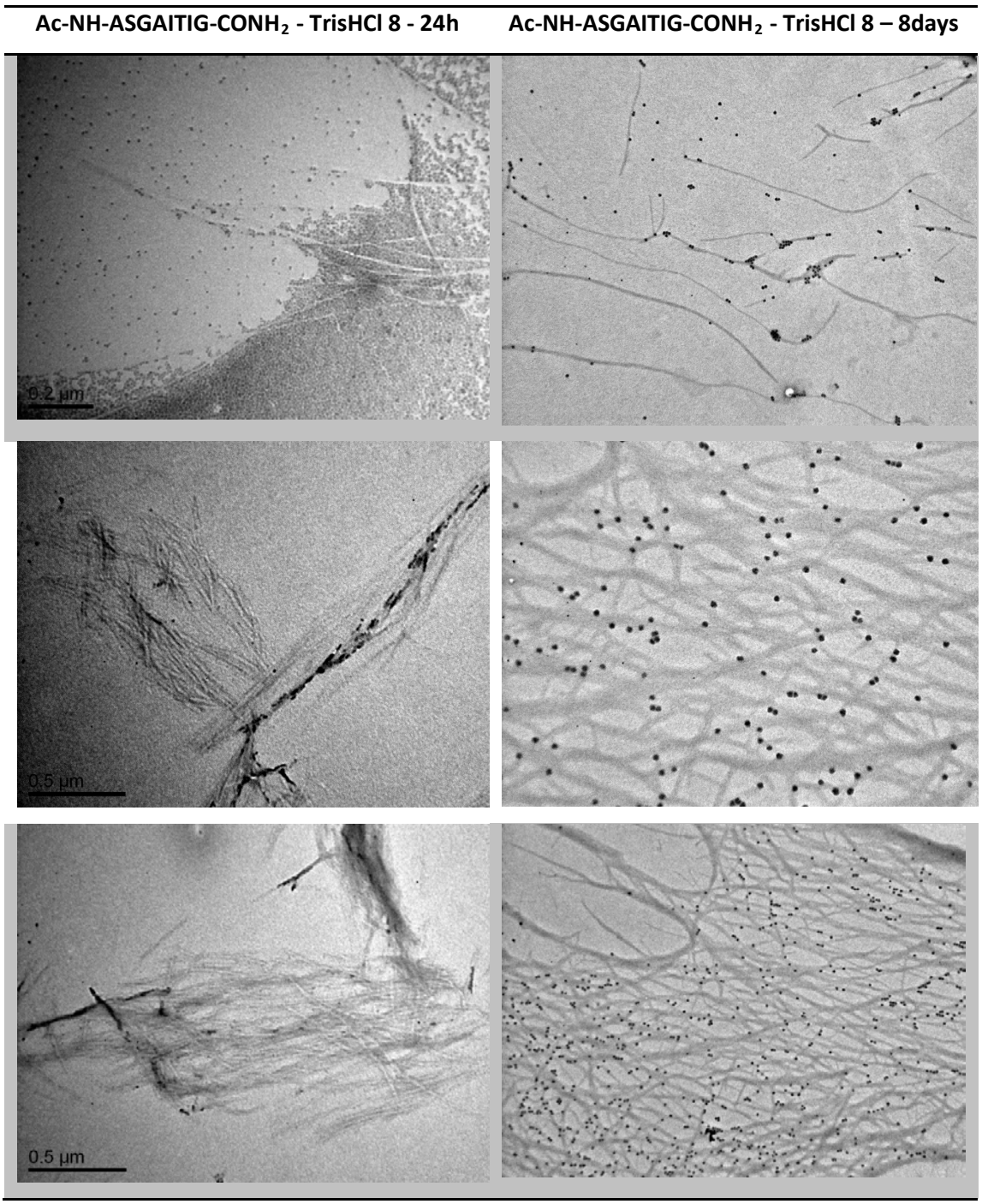

Fig. 7.11 Transmission Electron Microscopy images of the Ac-NH-ASGAITIG-$CONH_2$ peptide fibrils in TrisHCl pH 8 after *in vitro* silicification for 24h (left column) and 8days (right column).

Ac-NH-ASGAITIG-$CONH_2$ (TrisHCl pH 8)

24 hours of silicification: Ac-NH-ASGAITIG-$CONH_2$ did not show any evidence of templating. Monodispersed silica nanoparticles of d=9±1nm were observed between fibrils.

8 days of silicification: a similar image was depicted after 8 days of incubation, where silica nanoparticles (d=14.7±3nm) were trapped in the fibrillar network.

Control sample (Tris pH 8)

Finally, the control sample of TrisHCl at pH 8 was exmined. The formed silica nanoparticles after 24 hours were monodispersed of diameter=8.7±2nm, while after 8 days they increased to d=11.3±1nm (fig. 7.12).

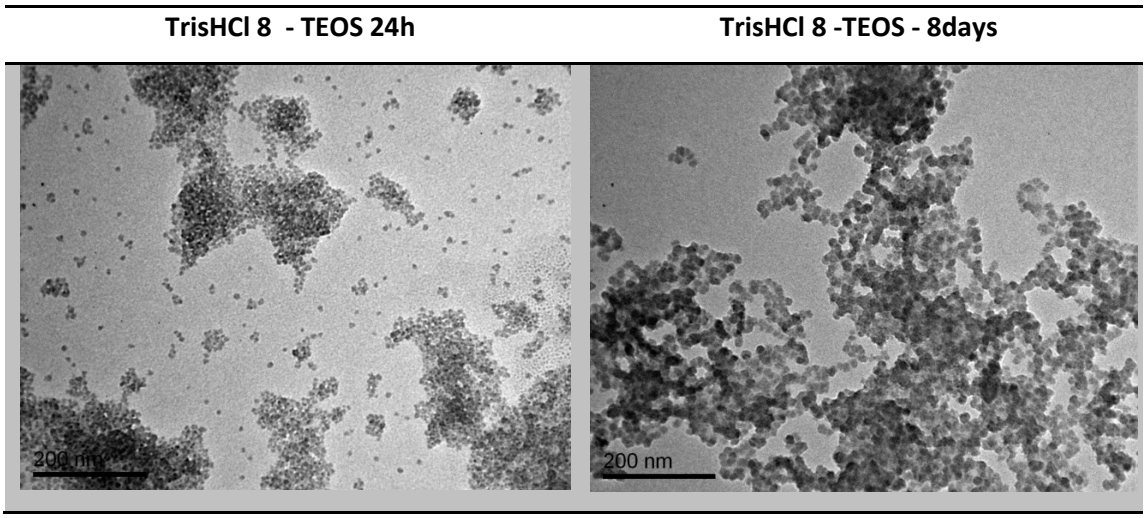

Fig. 7.12 TEOS hydrolysis and formation of particles in the absence of peptides in TrisHCl pH 8.

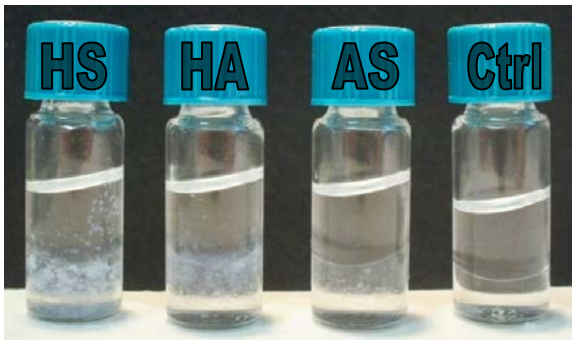

Fig. 7.13 Ac-NH-ASGAITIG-$CONH_2$, Ac-NH-ASGAITIG-$CONH_2$ and Ac-NH-ASGAITIG-$CONH_2$ in TrisHCl pH 8 after 8 days of incubation with TEOS.

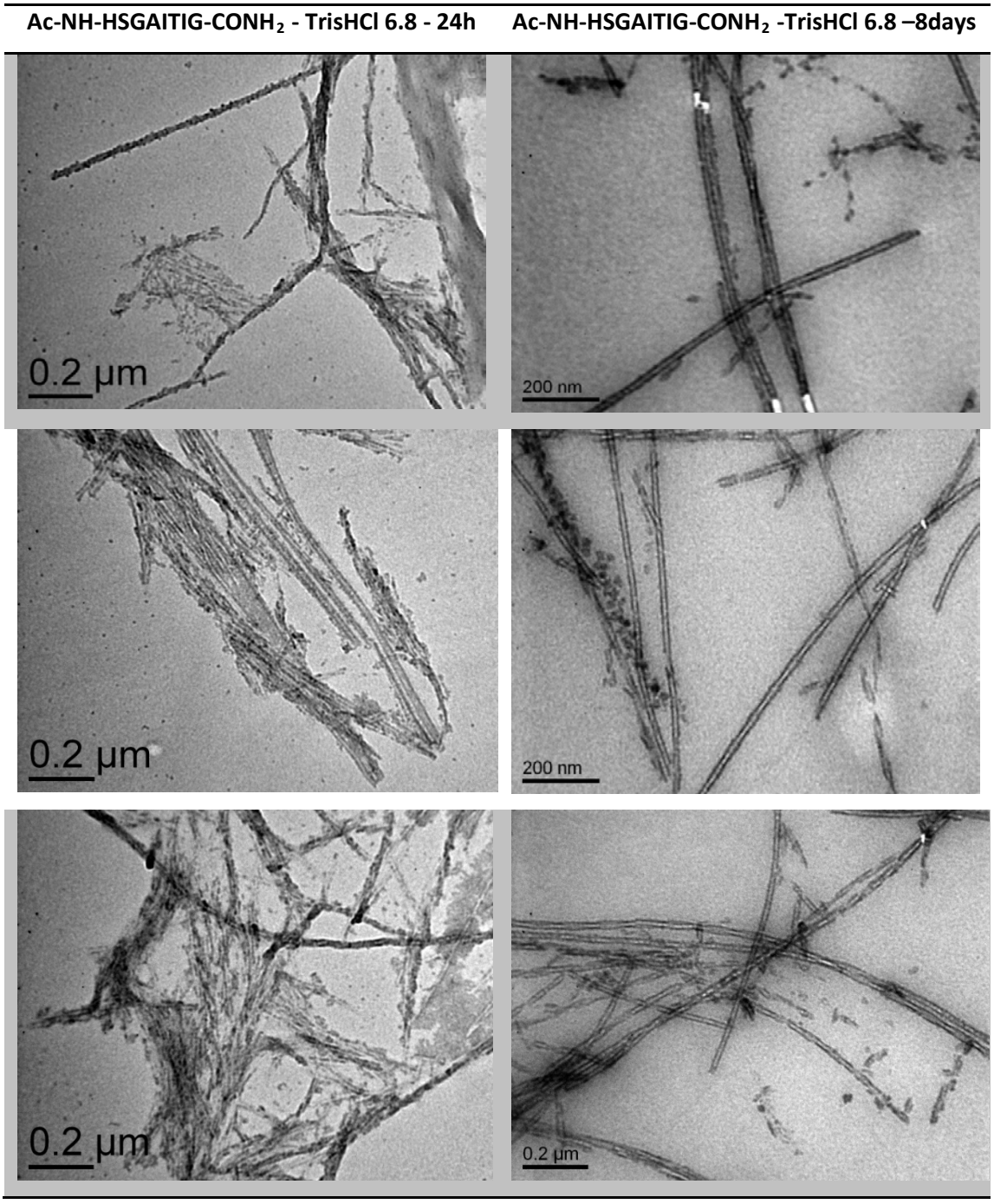

Fig. 7.14 Transmission Electron Microscopy images of the Ac-NH-HSGAITIG-$CONH_2$ peptide fibrils in TrisHCl pH 6.8 after *in vitro* silicification for 24h (left column) and 8days (right column).

Ac-NH-HSGAITIG-$CONH_2$ (TrisHCl pH 6.8)

24 hours of silicification: HS fibrils were covered by a thin layer of silica (l=4±1nm), while a very small number of free silica nanoparticles (d=8.1±2nm) was observed.

8 days of silicification: the deposition of silica was continued since fibrils were covered by a uniform thicker layer of l=6±1nm. No silica nanoparticles were observed.

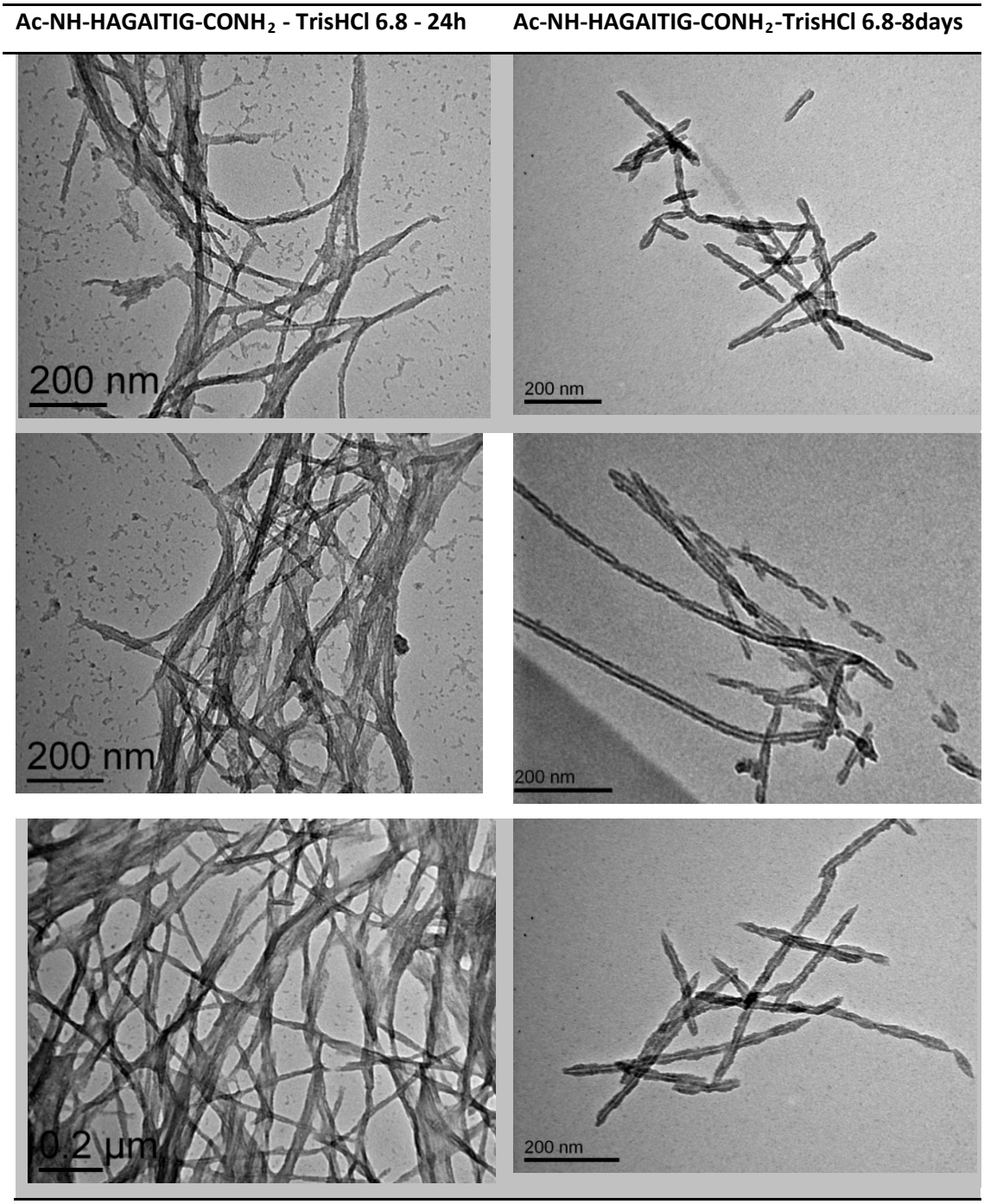

Fig. 7.15 Transmission Electron Microscopy images of the Ac-NH-HAGAITIG-$CONH_2$ peptide fibrils in TrisHCl pH 6.8 after *in vitro* silicification for 24h (left column) and 8days (right column).

Ac-NH-HAGAITIG-$CONH_2$ (Tris pH 6.8)

24 hours of silicification: HA fibrils were coated by a thin layer of silica (l=4.6±2nm), while a very small number of silica nanoparticles was observed.

8 days of silicification: the layer of deposited silica upon HA fibrils was increased to l=6.1±1nm. No silica nanoparticles were observed.

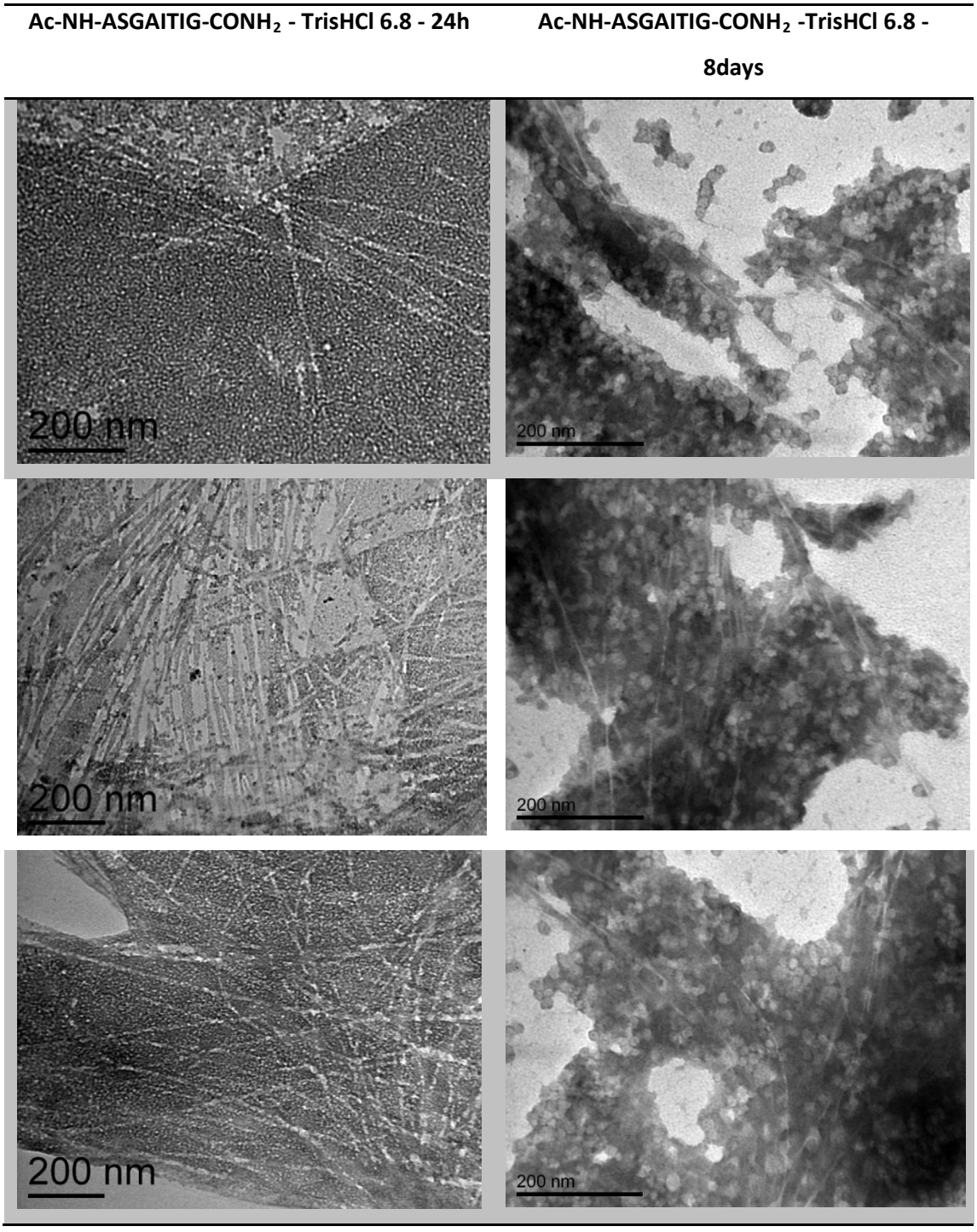

Fig. 7.16 Transmission Electron Microscopy images of the Ac-NH-ASGAITIG-$CONH_2$ peptide fibrils in TrisHCl pH 6.8 after *in vitro* silicification for 24h (left column) and 8days with negative staining (right column).

Ac-NH-ASGAITIG-$CONH_2$ (TrisHCl pH 6.8)

24 hours of silicification: AS fibrils coexisted with silica nanoparticles of d=4.2nm, without showing any kind of template.

8 days of silicification: After sonication and washing all silica nanoparticles were removed from the solution and moreover the fibrillar network was collapsed. Thus the depiction of fibrils was very difficult without negative staining, which finally showed that fibrils did not template silica nanoparticles.

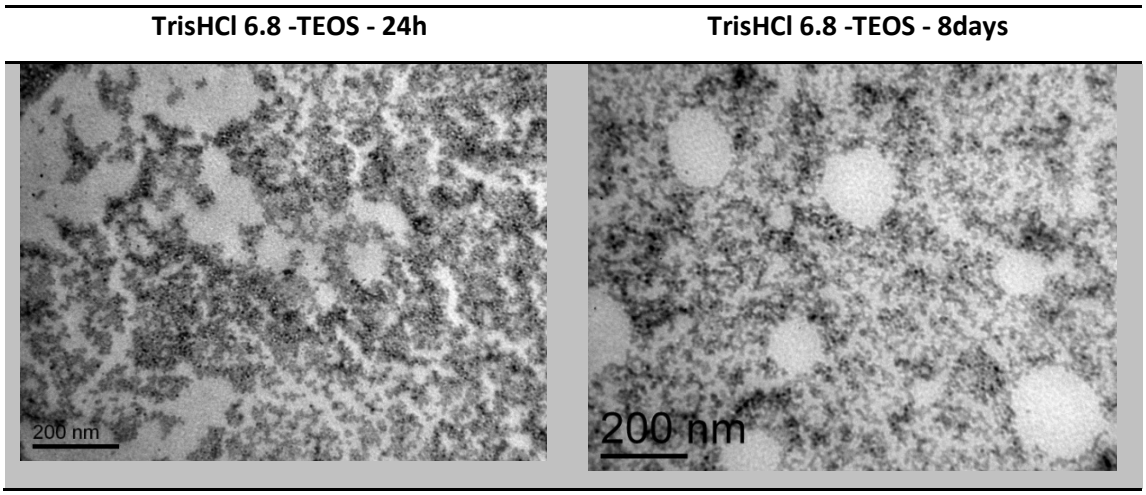

Fig. 7.17 TEOS hydrolysis and formation of particles in the absence of peptides in TrisHCl pH 6.8.

Control (Tris pH 6.8)

The hydrolysis of TEOS in TrisHCl pH 6.8 resulted in silica nanoparticles of d= 6±1nm.

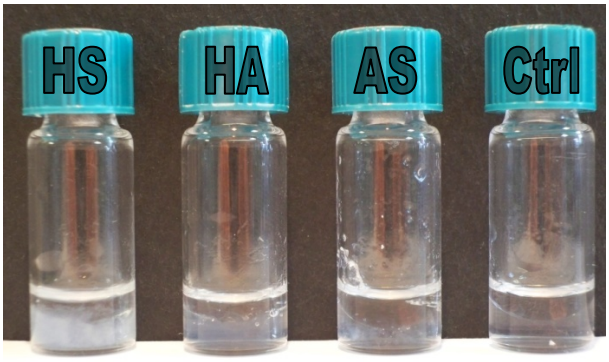

Fig. 7.18 Ac-NH-HSGAITIG-$CONH_2$, Ac-NH-HAGAITIG-$CONH_2$ and Ac-NH-ASGAITIG-$CONH_2$ in TrisHCl pH 6.8 after 8 days of incubation with TEOS.

The morphology of templated Ac-NH-HSGAITIG-$CONH_2$ was also examined by a field-emission scanning electron microscope which confirmed that the silica deposition follows the underlying fibril template. In particular, the twisted ribbon morphology is evident for the HS templated fibrils.

Ac-NH-HSGAITIG-CONH$_2$ - TrisHCl 8 - 8days

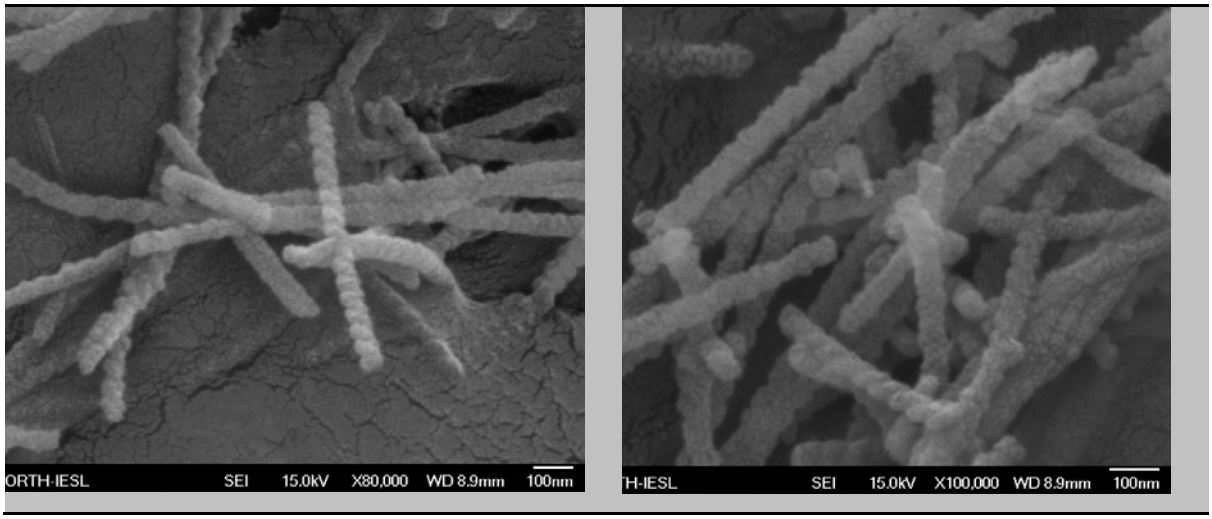

Fig. 7.19 FESEM image of Ac-NH-HSGAITIG-CONH$_2$ in TrisHCl pH 8 after 8days of incubation.

Ac-NH-HAGAITIG-CONH$_2$ - TrisHCl 8 - 8days

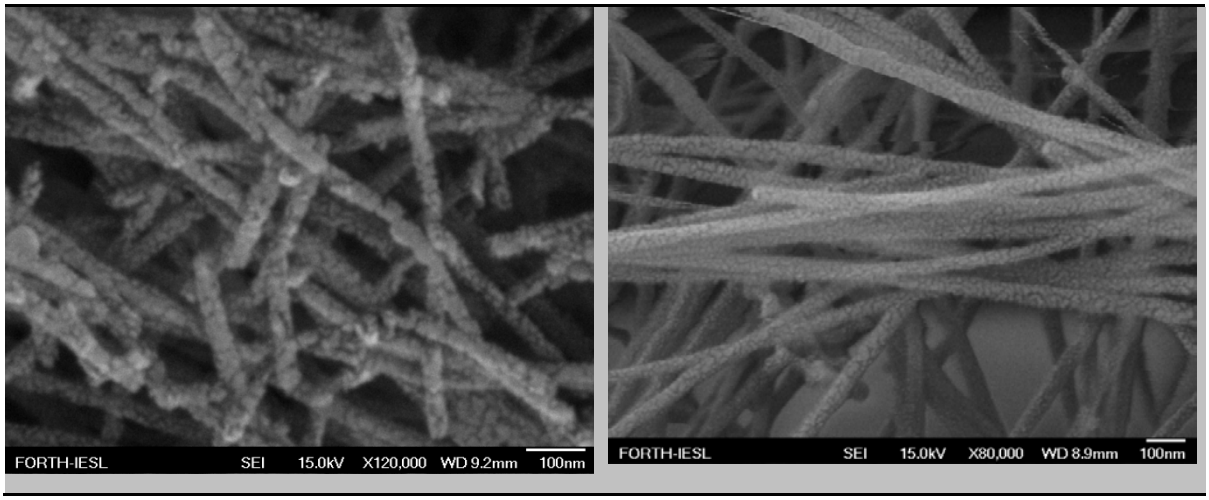

Fig. 7.20 FESEM image of Ac-NH-HAGAITIG-CONH$_2$ in TrisHCl pH 8 after 8days of incubation.

Ac-NH-ASGAITIG-CONH$_2$ - TrisHCl 8 - 8days

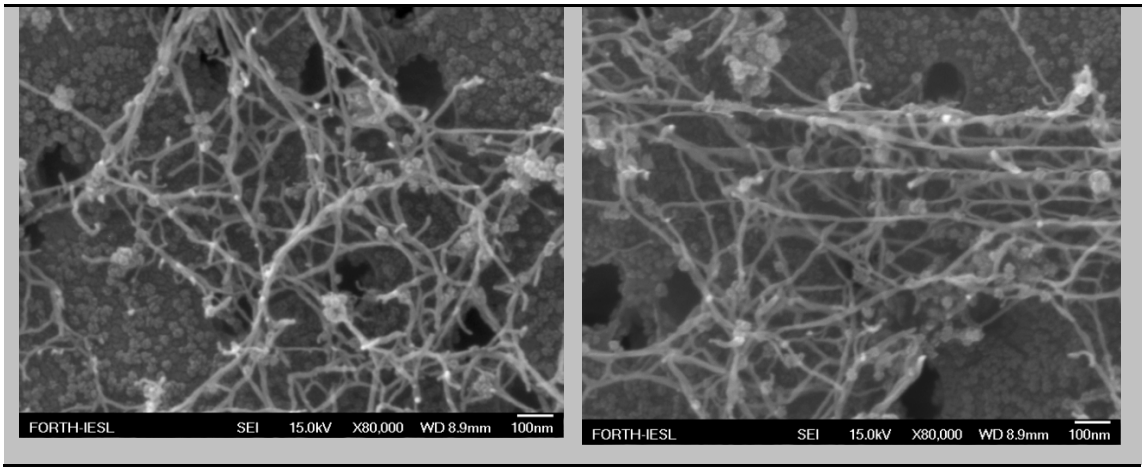

Fig. 7.21 FESEM image of Ac-NH-ASGAITIG-CONH$_2$ in TrisHCl pH 8 after 8days of incubation.

CHAPTER 8 Discussion and perspectives

In the context of the present thesis we demonstrated the ability of histidine and serine containing amyloid-like peptides to act as templates for silica nanoparticles. More precisely we focused on:

1. The design and structural characteristics of self-assembling peptides originating from the adenovirus protein and
2. Their interaction with silica precursors.

During the first part of our experiments we showed that the peptides Ac-NH-HSGAITIG-$CONH_2$, Ac-NH-HAGAITIG-$CONH_2$ and of Ac-NH-ASGAITIG-$CONH_2$ can self-assemble into a fibrillar amyloid-like hydrogel in Tris-HCl buffer of pH 6.8 and 8. TEM images showed that all fibrils had an amyloid-like twisted morphology, of d= 3.84nm that could reach the order of microns and pitch 22.7nm. RAMAN measurements also confirmed the existence of the characteristic β-sheet peak of amyloid-like fibrils.

The pKa of the histidine containing peptides of Ac-NH-HSGAITIG-$CONH_2$ and of Ac-NH-HAGAITIG-$CONH_2$ were determined by titration and were found to be 6.28.

In the second part of our experiments we studied the interaction of fibrils with TEOS precursor using TEM and FESEM techniques. We have investigated this interaction at two pH values) at pH 8, where the peptides do not carry any charge, and at pH 6.8, slightly above the pK values of the peptide's histidines. A) in pH 8 the peptide Ac-NH-HSGAITIG-$CONH_2$ was found to template the formation of silica nanoparticles. Since His is deprotonated, the nitrogen of imidazole group has a lone electron pair which allows it to act as good hydrogen acceptor of the Ser hydroxyl group. In that way Ser becomes a better nucleophile and it attacks the silicon precursor leading to the formation of a silanol molecule. Thus the Serine residues act as nucleation points for silica precursors that further condense on the surface of the fibrils resulting to the formation of almost monodisperse silica nanoparticles. In the case of pH 6.8 silica deposition is more complicated, since protonated and deprotonated His residues coexist. At this pH, a tubular silica layer surrounds the fibril surface and monidispersed nanoparticles templated on fibrils are scarcely observed. We assume that the protonated His reacts electrostatically with the negatively charged silica nanoparticles (which are formed due to their reaction with water) and they are deposited in a uniform layer. The peptide Ac-NH-HAGAITIG-$CONH_2$ at pH 8 did not present any silica deposition presumably, due to the absence of the nucleophile Serine residue. However, it templated

silica in pH 6.8, presumably due to the electrostatic interactions mediated by histidines. Finally, the peptide Ac-NH-ASGAITIG-$CONH_2$ was the only peptide which did not template silica nanoparticles in both pHs. At pH 8 this can be attributed to the absence of the histidine residue that renders serine nucleophilic, and in pH 6.8 to the absence of any positively charged residues on its surface to attract negatively charged silica precursors.

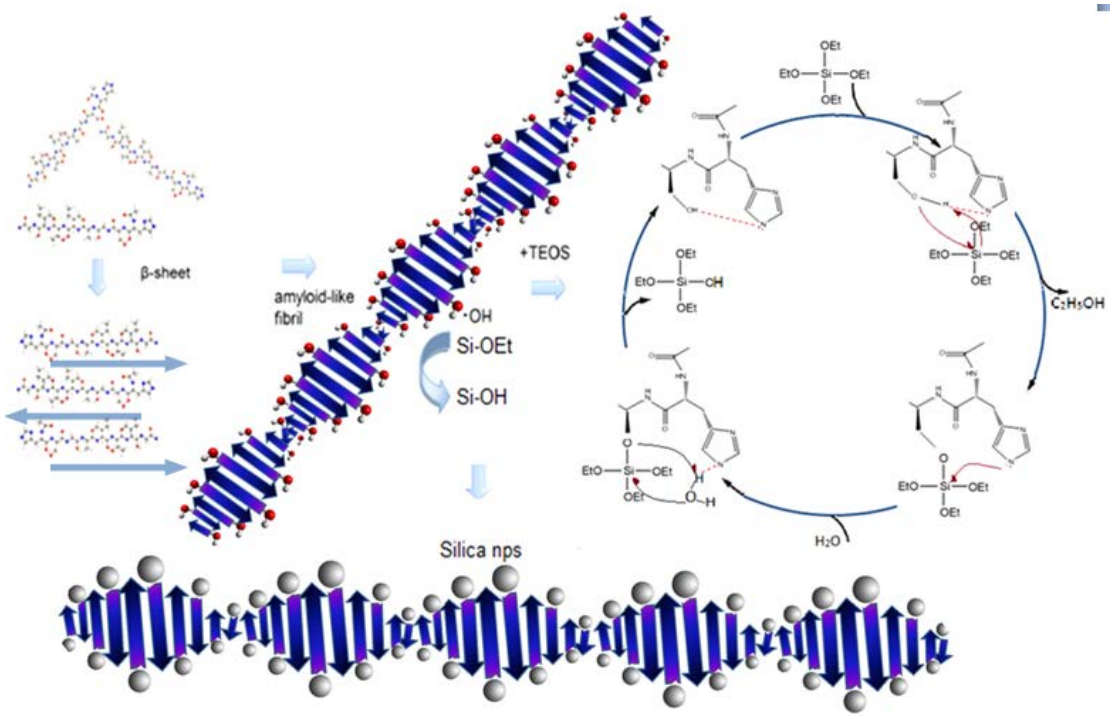

Fig. 8.1 Schematic representation of the formation of amyloid-like fibril from the peptide Ac-NH-HSGAITIG-$CONH_2$ and silica template.

Moreover, the peptide Ac-NH-ASGAITIG-$CONH_2$ fibrils adopts twisted morphologies, and the deposition of silica nanoparticles follows the underlying fibril template, resulting in "pearl necklace" morphologies.

In summary, we demonstrated the ability of serine and histidine containing self-assembling peptides to act as templates for silica deposition. Such self-assembling systems present advantages relatively to polymer or other organic templates due to their biocompatibility, biodegrability and ability to gel at near physiological pH.

These properties enable our system for several biomedical applications. Peptide-silica hydrogels could be used as a bone replacement material, as a scaffold of tissue engineering or as a coating for metal implants.

Appendix

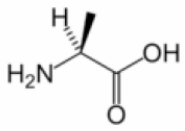 L-Alanine (Ala / A)	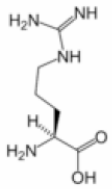 L-Arginine (Arg / R)	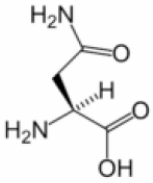 L-Asparagine (Asn / N)	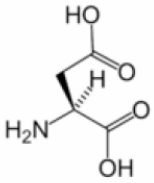 L-Aspartic acid (Asp / D)	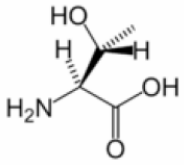 L-Threonine (Thr / T)
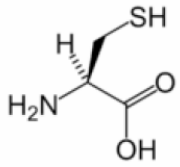 L-Cysteine (Cys / C)	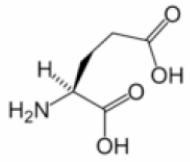 L-Glutamic acid (Glu / E)	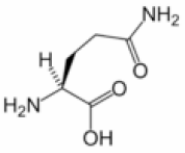 L-Glutamine (Gln / Q)	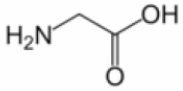 Glycine (Gly / G)	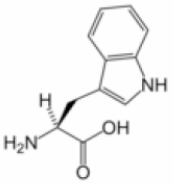 L-Tryptophan (Trp / W)
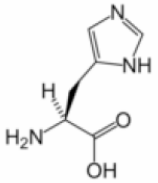 L-Histidine (His / H)	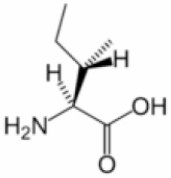 L-Isoleucine (Ile / I)	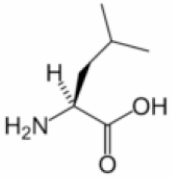 L-Leucine (Leu / L)	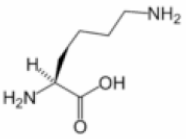 L-Lysine (Lys / K)	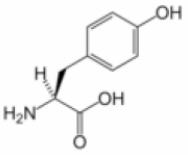 L-Tyrosine (Tyr / Y)
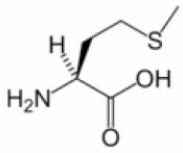 L-Methionine (Met / M)	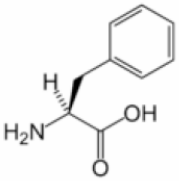 L-Phenylalanine (Phe / F)	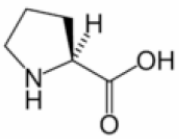 L-Proline (Pro / P)	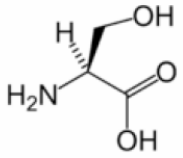 L-Serine (Ser / S)	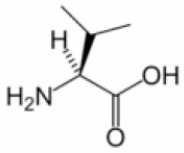 L-Valine (Val / V)

Structures and symbols of the 20 amino acids, which are directly encoded for protein synthesis by the standard genetic code.

CHAPTER 9 – References

Adamson, D. H., D. M. Dabbs, et al. (2007). "Non-peptide polymeric silicatein alpha mimic for neutral pH catalysis in the formation of silica." Macromolecules 40(16): 5710-5717.

Altunbas, A., N. Sharma, et al. "Peptide-Silica Hybrid Networks: Biomimetic Control of Network Mechanical Behavior." Acs Nano 4(1): 181-188.

Brutchey, R. L. and D. E. Morse (2008). "Silicatein and the Translation of its Molecular Mechanism of Biosilicification into Low Temperature Nanomaterial Synthesis." Chemical Reviews 108(11): 4915-4934.

Cha, J. N., K. Shimizu, et al. (1999). "Silicatein filaments and subunits from a marine sponge direct the polymerization of silica and silicones in vitro." Proceedings of the National Academy of Sciences of the United States of America 96(2): 361-365.

Gilead, S. and E. Gazit (2005). "Self-organization of short peptide fragments: From amyloid fibrils to nanoscale supramolecular assemblies." Supramolecular Chemistry 17(1-2): 87-92.

Haines-Butterick, L., K. Rajagopal, et al. (2007). "Controlling hydrogelation kinetics by peptide design for three-dimensional encapsulation and injectable delivery of cells." Proceedings of the National Academy of Sciences of the United States of America 104(19): 7791-7796.

Hennink, W. E. and C. F. van Nostrum (2002). "Novel crosslinking methods to design hydrogels." Advanced Drug Delivery Reviews 54(1): 13-36.

Iler, R. K. (1980). "ISOLATION AND CHARACTERIZATION OF PARTICLE NUCLEI DURING THE POLYMERIZATION OF SILICIC-ACID TO COLLOIDAL SILICA." Journal of Colloid and Interface Science 75(1): 138-148.

Kasotakis, E., E. Mossou, et al. (2009). "Design of Metal-Binding Sites Onto Self-Assembled Peptide Fibrils." Biopolymers 92(3): 164-172.

Kayed, R., J. Bernhagen, et al. (1999). "Conformational transitions of islet amyloid polypeptide (IAPP) in amyloid formation in vitro." Journal of Molecular Biology 287(4): 781-796.

Kisailus, D., J. H. Choi, et al. (2005). "Enzymatic synthesis and nanostructural control of gallium oxide at low temperature." Advanced Materials 17(3): 314-+.

Knecht, M. R. and D. W. Wright (2003). "Functional analysis of the biomimetic silica precipitating activity of the R5 peptide from Cylindrotheca fusiformis." Chemical Communications(24): 3038-3039.

Kroger, N., R. Deutzmann, et al. (1999). "Polycationic peptides from diatom biosilica that direct silica nanosphere formation." Science 286(5442): 1129-1132.

Luckey, M., J. F. Hernandez, et al. (2000). "A peptide from the adenovirus fiber shaft forms amyloid-type fibrils." Febs Letters 468(1): 23-27.

Meegan, J. E., A. Aggeli, et al. (2004). "Designed self-assembled beta-sheet peptide fibrils as templates for silica nanotubes." Advanced Functional Materials 14(1): 31-37.

Naik, R. R., P. W. Whitlock, et al. (2003). "Controlled formation of biosilica structures in vitro." Chemical Communications(2): 238-239.

Papanikolopoulou, K., G. Schoehn, et al. (2005). "Amyloid fibril formation from sequences of a natural beta-structured fibrous protein, the adenovirus fiber." Journal of Biological Chemistry 280(4): 2481-2490.

Papanikolopoulou, K., S. Teixeira, et al. (2004). "Adenovirus fibre shaft sequences fold into the native triple beta-spiral fold when N-terminally fused to the bacteriophage T4 fibritin foldon trimerisation motif." J Mol Biol 342(1): 219-27.

Perry, C. C. and T. Keeling-Tucker (2000). "Biosilicification: the role of the organic matrix in structure control." Journal of Biological Inorganic Chemistry 5(5): 537-550.

Reches, M. and E. Gazit (2003). "Casting metal nanowires within discrete self-assembled peptide nanotubes." Science 300(5619): 625-627.

Roth, K. M., Y. Zhou, et al. (2005). "Bifunctional small molecules are biomimetic catalysts for silica synthesis at neutral pH." Journal of The American Chemical Society 127(1): 325-330.

Serpell, L. C. (2000). "Alzheimer's amyloid fibrils: structure and assembly." Biochimica Et Biophysica Acta-Molecular Basis of Disease 1502(1): 16-30.

Shimizu, K., J. Cha, et al. (1998). "Silicatein alpha: Cathepsin L-like protein in sponge biosilica." Proceedings of the National Academy of Sciences of the United States of America 95(11): 6234-6238.

Sipe, J. D. and A. S. Cohen (2000). "Review: History of the amyloid fibril." Journal of Structural Biology 130(2-3): 88-98.

Sumper, M. and E. Brunner (2006). "Learning from diatoms: Nature's tools for the production of nanostructured silica." Advanced Functional Materials 16(1): 17-26.

Tamamis, P., E. Kasotakis, et al. (2009). "Amyloid-Like Self-Assembly of Peptide Sequences from the Adenovirus Fiber Shaft: Insights from Molecular Dynamics Simulations." Journal of Physical Chemistry B 113(47): 15639-15647.

Tenidis, K., M. Waldner, et al. (2000). "Identification of a penta- and hexapeptide of islet amyloid polypeptide (IAPP) with amyloidogenic and cytotoxic properties." J Mol Biol 295(4): 1055-71.

van Raaij, M. J., A. Mitraki, et al. (1999). "A triple beta-spiral in the adenovirus fibre shaft reveals a new structural motif for a fibrous protein." Nature 401(6756): 935-938.

Wang, S. J., X. Ge, et al. (2011). "Mechanistic Processes Underlying Biomimetic Synthesis of Silica Nanotubes from Self-Assembled Ultrashort Peptide Templates." Chemistry of Materials 23(9): 2466-2474.

Westermark, P., C. Wernstedt, et al. (1987). "AMYLOID FIBRILS IN HUMAN INSULINOMA AND ISLETS OF LANGERHANS OF THE DIABETIC CAT ARE DERIVED FROM A NEUROPEPTIDE-LIKE PROTEIN ALSO PRESENT IN NORMAL ISLET CELLS." Proceedings of the National Academy of Sciences of the United States of America 84(11): 3881-3885.

Wright, C. F., S. A. Teichmann, et al. (2005). "The importance of sequence diversity in the aggregation and evolution of proteins." Nature 438(7069): 878-881.

Zhang, J. X., A. Skardal, et al. (2008). "Engineered extracellular matrices with cleavable crosslinkers for cell expansion and easy cell recovery." Biomaterials 29(34): 4521-4531.

Zhang, S. G. (2003). "Fabrication of novel biomaterials through molecular self-assembly." Nature Biotechnology 21(10): 1171-1178.

Heinz C. Schroder, Matthias Wiens, Xiaohong Wang, Ute Schloßmacher and Werner E.G. Muller, (2011) "Biosilica-Based Strategies for Treatment of Osteoporosis and Other Bone Diseases"

Book references

Nelson David and Michael Cox. (2000). *"Principles of Biochemistry" Lehninger Principles of Biochemistry, 3rd Edition*. New York: Wort

Yoon S. Lee (2008). "SELF-ASSEMBLY AND NANOTECHNOLOGY A Force Balance Approach", Wiley publications.

Donald Voet, Judith G. Voet, Charlotte W. Pratt (2009), "Principles of Biochemistry", 3rd Edition International

Heinz C. Schröder, Ute Schloßmacher, Alexandra Boreiko, Filipe Natalio, Malgorzata Baranowska, David Brandt, Xiaohong Wang, Wolfgang Tremel, Matthias Wiens, and Werner E.G. Müller, (2009), "Silicatein: Nanobiotechnological and Biomedical Applications"

Internet references

http://www.ebi.ac.uk/interpro/IEntry?ac=IPR002049)

http://www.biocompare.com/Application-Notes/118761-The-Direct-Detect-Biomolecular-Quantitation-System/